Studies of High Temperature Superconductors, *edited by A.V. Narlikar, NOVA Science Publishers, New York*, 2001, vol 39, pp 213-244

FLUX FLOW OSCILLATORS FOR SUPERCONDUCTING INTEGRATED SUBMM WAVE RECEIVERS

Valery P. Koshelets and Jesper Mygind*

Institute of Radio Engineering and Electronics, Russian Academy of Science, Mokhovaya 11, GSP-9, 101999, Moscow, Russia; Space Research Organization of the Netherlands (SRON), P.O. Box 800, 9700 AV Groningen, the Netherlands

****Department of Physics, Technical University of Denmark, B 309, DK-2800 Lyngby, Denmark***

1. INTRODUCTION

Lightweight and compact ultra-sensitive submm Superconducting Integrated Receiver (SIR) [1] with low power consumption is very attractive for both radio-astronomical research and remote monitoring of the Earth atmosphere. The new ambitious radio-astronomy multi-dish projects (e.g. ALMA) would gain considerably by using single-chip SIRs due to their lower price and better serviceability as compared to conventional approaches. A remote study of the atmospheric pollution is possible using air- or satellite borne SIRs for detection of the spectrum lines of ozone, chlorine and other elements in the submm wave range. Presently the single-chip superconducting receiver comprises a SIS-mixer with quasioptical antenna and a superconducting local oscillator.

The SIS mixer is the most sensitive detector element for heterodyne reception in the frequency range 100 - 1000 GHz [1-7]. SIS receivers are being used successfully in radio astronomy for observation of spectra showing the lowest noise temperature in the mm and sub-mm wave range. The noise temperature of a SIS receiver is ultimately limited only by the fundamental quantum value hf/2k. Many applications lack a compact and easily tunable submm local oscillator (LO), the direct integration of a superconducting LO with the SIS mixer offers a real breakthrough. Presently, mainly two kinds of superconducting oscillators are under investigation: arrays of lumped Josephson junctions and distributed flux-flow oscillators (FFOs).

Several types of Josephson one-dimensional (1-D) and two-dimensional (2-D) arrays have been proposed and studied [8-18], most of them are based on overdamped Josephson junctions (JJ) with non-hysteretic current-voltage characteristics (IVC). Series connected 1-D arrays have been investigated for many years; recent designs combine compact groups of JJs placed with half wavelength distance in a microstrip transmission line [8-12]. Power

as high as 0.85 mW near 240 GHz has been detected in a matched load at an optimal (internal resonance) frequency [10]. Radiation from the linear array oscillator was measured both by an on-chip integrated detector and by sensors placed outside the test cryostat. Typically the maximum operational frequency was about 300 GHz [8-10] limited by the internal plasma frequency and the LC resonance frequency of the shunt resistor. In order to extend this limit up to 1 THz a new shunted junction with a small parasitic inductance of about 100 fH has been developed [11,12]. The inductance was minimized by reducing the inductive length between the tunnel junction and a contact hole to about 1 μm. As a result power up to 10 μW at 625 GHz has been delivered to the integrated load. A combined linewidth of two 1-D JJ oscillators of about 8 MHz was measured at 566 GHz. However, considerable variation of the JJ array output power over the frequency range makes a direct implementation of the existing JJ array into integrated receivers rather problematic, especially taking into account the lack of an "internal" mechanism to adjust the emitted power. However, for this purpose an on-chip integrated superconducting attenuator [19] with electronic tuning has been proposed. The device employs the dependence of the SIS junction quasi-particle curve on the amplitude of the applied rf current. This attenuator has a frequency range of about 10%, a dynamic range of a few dB (the lower frequency, the wider dynamic range), but is limited to a few μW saturation level.

Many different designs of the 2-D arrays have been tested [13-18]; some of which demonstrated acceptable frequency tuning - from 100 to 250 GHz [13] -, and very efficient dc/rf power conversion - up to 30% for a 2D-array of underdamped JJs [18]. Nevertheless, taking into account all the requirements for integration of the LO into the integrated superconducting submm receiver, the existing JJ array oscillators do not appear suitable for real applications.

At the moment the Flux Flow Oscillator (FFO) based on the unidirectional flow of magnetic vortices in a long Josephson tunnel junction [20] is the best choice for integration with an SIS mixer. Local oscillators based on Nb-AlO_x-Nb FFOs have been successfully tested from about 120 to 700 GHz (gap frequency of Nb) providing power enough to pump an SIS-mixer (about 1 μW at 450 GHz); both the frequency and the power of the FFO can be dc tuned [21, 22]. A front-end noise temperature of 85 K has been achieved at 140 GHz for a waveguide integrated receiver with a FFO as local oscillator [23]. Progress in the development of the quasi-optical integrated receiver with a FFO [24, 25] was presented in the recent review [1]. Just a few important points are worth to be mentioned. i) A receiver DSB noise temperature below 100 K has been achieved for SIR with the internal FFO operated in the frequency range 480 - 520 GHz [26]; it means that the performance of the SIS mixer is close to the quantum limit. ii) A free-running FFO linewidth considerably below 1 MHz has been measured near 450 GHz [27, 28]. Furthermore, phase locking of the Josephson FFO to an external oscillator has recently been demonstrated experimentally [28], and a linewidth as low as 1 Hz (determined by the resolution bandwidth of the spectrum analyzer) was measured relative to a reference oscillator in the frequency range 270 - 440 GHz. iii) The FFO can be fabricated on the same trilayer (and by using the same technological procedure) as the SIS mixer; and furthermore the circuit complexity of the FFO is much lower than the JJ array oscillator.

In this paper an overview of the FFO properties [1, 21-25, 27, 28] will be presented along with the latest results for the FFO radiation linewidth measurements and phase locking of the FFO to an external reference oscillator.

2. PROPERTIES OF FLUX FLOW OSCILLATORS.

The FFO is a *long* Josephson tunnel junction in which an applied dc magnetic field and a dc bias current, I_B, drive a unidirectional flow of fluxons, each containing one magnetic flux quantum, $\Phi_0 = h/2e \approx 2\ 10^{-15}$ Wb. Symbol h is Planck's constant and e is the elementary charge. An external coil or an integrated control line with current I_{CL} can be used to generate the dc magnetic field applied to the FFO. According to the Josephson relation the junction biased at voltage V oscillates with a frequency $f = (1/\Phi_0)*V$ (about 483.6 GHz/mV). The velocity and density of the fluxons and thus the power and frequency of the emitted mm-wave signal may be adjusted independently by both the bias current and the magnetic field.

Long Josephson Nb-AlO_x-Nb junctions with overlap geometry are used as FFOs (see inset in figure 1). The FFO length, L, and the width, W, are about 500 μm and 3 μm, respectively. The value of the critical current density, j_c, is in the range 2 - 8 kA/cm^2 giving a Josephson penetration depth, $\lambda_J \approx 8$ - 4 μm. The corresponding specific resistance, $R_n*L*W \approx 100$ - 25 Ω μm^2. For the numerical calculations we use typical values of the London penetration depth ($\lambda_L \approx 90$ nm) and the junction specific capacitance ($C_s \approx 0.08$ pF/μm^2). The active area of the FFO (i. e. the AlO_x tunnel barrier) is usually formed in a long window in the relatively thick insulation layer (200-350 nm, SiO_2) between two superconducting (Nb) films (base and counter electrodes). The so-called "idle" region in the thick SiO_2 layer between the overlapping electrodes adjacent to the junction forms a transmission line parallel to the FFO. The width of the idle region is about the junction width ($W_i \approx 3$ μm), which is limited by the alignment accuracy of the fabrication process. One of the electrodes of FFO is employed as a control line in which a dc current, I_{CL}, produces the applied magnetic field, B_{appl}.

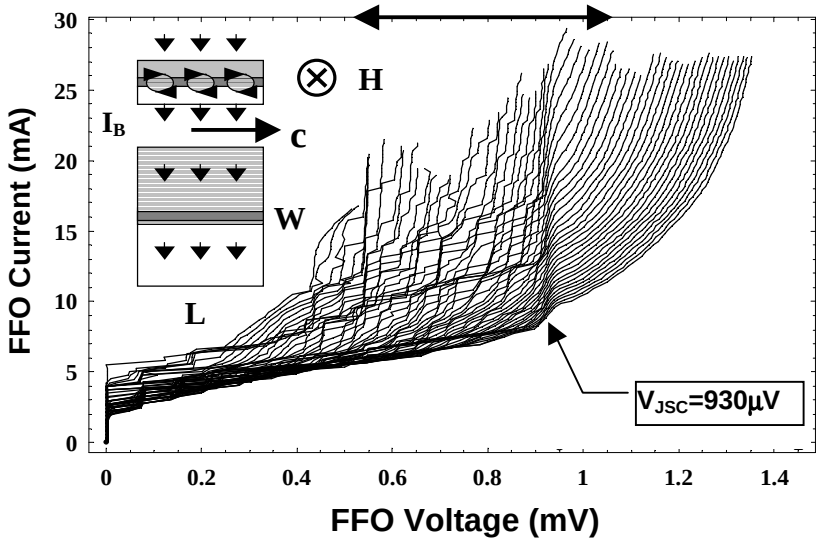

Fig. 1. Typical set of IVCs for a Nb-AlO_x-Nb FFO recorded with incremented magnetic fields. Each IVC is measured for a fixed control line current, I_{CL} which is then incremented by $\Delta I_{CL} \approx 0.5$ mA before the next IVC is recorded. Note the abrupt change of the IVC at the boundary voltage $V_{JSC} \approx 930$ μV, above which the voltage and thus the frequency of the FFO increases linearly with ΔI_{CL} (for fixed bias current I_B). The various regimes are discussed in the text. Insets show the cross section of the long junction with driven vortices (top) and its overlap geometry (bottom).

2.1 Frequency and power tuning.

A special integrated circuit comprising a well-coupled wide-band SIS detector is used to characterize the FFO as an rf source. Figure 1 shows a typical set of current-voltage characteristics (IVCs) of the FFO measured with incremented magnetic fields. Each IVC is recorded with a fixed control line current, I_{CL}, which is subsequently increased with a constant increment ΔI_{CL}. Simultaneously with the recording of the FFO IVCs, the pumped IV curves of the integrated SIS detector were measured by a newly developed data collection system (IRTECON) [29]. The voltage range where the FFO delivers sufficient power to pump the integrated SIS detector is marked on the top voltage axis in figure 1. The magnitude of the pump signal is derived from the induced change in the subgap tunnel current, ΔI, of the SIS detector at V = 2 mV due to photon assistant tunneling normalized to the current rise, I_g, at the gap voltage. A ratio $\Delta I/I_g$ of more than 0.25 is obtained for FFO voltages from 550 to 1070 μV (see figure 1) corresponding to the frequency range 270-520 GHz. IVCs of the SIS detector recorded at different setting of the FFO are shown in figure 2 [21]. Pronounced quasiparticle steps are clearly visible in the SIS IVC up to a FFO frequency of 665 GHz. Actually the useful frequency range is limited by the matching circuits and the SIS tuning structure rather than by the FFO itself. It is possible to change the frequency range of the integrated circuit by modifying the design of the matching elements. Implementation of a FFO based on superconductors with a higher critical temperature (higher gap voltage) results in a considerable increase of the maximum operational frequency. Recently excitation of the resonances by Josephson radiation at frequencies up to 1.5 THz has been demonstrated [30] for NbN and NbC_xN_{1-x} tunnel junctions.

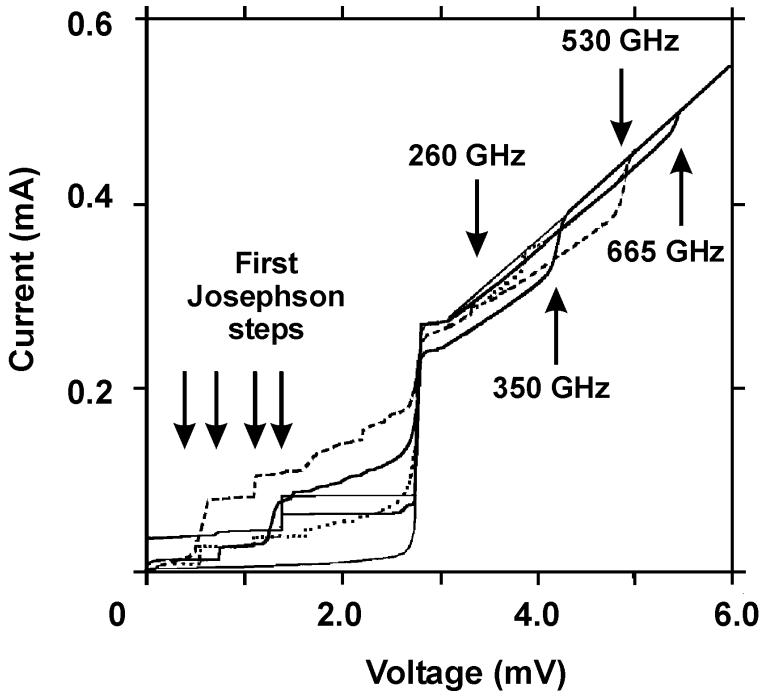

Fig. 2. [21] IVCs of the SIS detector (wide band design) pumped by a FFO at different frequencies. The arrows point to the quasi-particle steps (photon assisted tunneling) and the first Shapiro steps for four FFO frequencies, 260, 350, 530 and 665 GHz.

Since the power and frequency of the emitted mm-wave signal may be adjusted independently, the FFO power can be precisely tuned at a fixed frequency. Curve "a" in figure 3 [31] shows the unpumped SIS IVC. The Josephson effect in the SIS junction is suppressed by a magnetic field generated by a dc current through the integrated control line, which as described is made in one of the electrodes of the junction. The IVCs of the SIS mixer pumped by the FFO operating at f = 470 GHz for two different power levels are curves "b" and "c" in figure 3. The normalized RF voltage, $\alpha = eV_{RF}/hf$ ($\alpha_b \approx 1.1$, $\alpha_c \approx 1.9$) is estimated by fitting the measured IVC to a numerically simulated IVC. From figure 3 one can see that the power provided by the FFO is sufficient to operate the SIS mixer. Furthermore, the FFO power can be continuously adjusted over a range of about 10 dB.

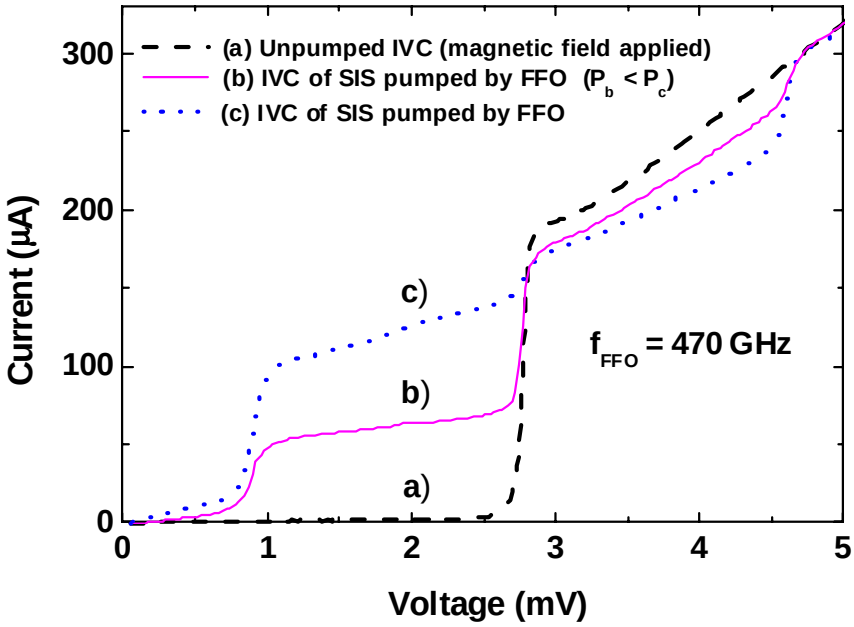

Fig. 3. [31] IVC of the SIS mixer: a) without FFO pump power; b) and c) pumped at two levels (P_b and P_c) of FFO power at 470 GHz (explained in text). The *ac* Josephson effect is suppressed by a magnetic field generated by the current in an integrated control line.

2.2 Regimes of FFO operation.

A thorough study of long Josephson junctions intended for wide-band integrated oscillators has been performed [32]. For small magnetic fields Zero Field Steps (ZFSs) were observed in the IVC of the FFO. The position of the ZFS is given by the length and the propagation velocity of electromagnetic waves along the FFO, the so-called Swihart velocity, c_{Sw}, which also is the maximum velocity of fluxons in the junction. The “idle” region in parallel to the junction has a much higher propagation velocity than that of the bare Josephson transmission line. This results in an increase of the effective Swihart velocity c_{Sw}^{eff} and consequently, the voltage of the ZFS, V_{ZFS}, is significantly increased. The value of c_{Sw}^{eff} which depends [33] on the ratio, W_i/W, between the width of the idle region and the junction is about 1.3 c_{Sw}.

The so-called Displaced Linear Slope (DLS) is observed in the IVC of the FFO at low magnetic fields. With increasing B_{appl} (see figure 1 at $V < 400$ μV) the DLS branch shifts almost linearly with B_{appl} towards higher voltages. When the FFO is biased within the DLS region, instead of the usual distinct superposition of quasi-particle and Shapiro steps, a "smearing" of the IVC of the SIS detector at $V \approx 0$ and $V \approx V_g$ was found [32]. This indicates that the FFO operates as a wide-band noise source while biased at DLS. Such behavior was reported for the first time in a paper [34], where an extremely broad radiation linewidth was observed for FFO biased at the DLS. Numerical simulations [34] showed that the FFO dynamics at the DLS is characterized by irregular fluxon oscillations that resemble a chaotic state. Qualitatively, the complicated fluxon dynamic can be attributed to excitation of the internal oscillation modes in the "soft" fluxon chain at weak magnetic fields.

At higher magnetic field the DLS transforms into the so-called flux-flow step (FFS) which at low internal FFO damping appear as [35] a series of resonant Fiske Steps (FS) as clearly seen in figure 1. In this region the FFO can only be biased in the narrow voltage ranges spanned by the individual FSs and thus the FFO only oscillates in the corresponding frequency intervals. This resonant mode exists up to a specific "boundary" voltage, V_{JSC}, where the FSs merge into a soft peak, that assembles the so-called Eck peak found in the infinitely long junction (velocity matching step). At the same voltage, V_{JSC}, a "bump" in dc current appears. As also seen from figure 1 for $V > V_{JSC}$, the FFS becomes smooth and with increasing I_{CL} the FFO voltage increases continuously proportional to the applied magnetic field, and persists up to the gap voltage. It should be noted that this "boundary" is typical for all investigated FFO with high current density ($j_c > 1$ kA/cm^2). This feature does not depend significantly neither on the exact junction geometry and its dimensions nor on the coupling to the external microwave circuits [32].

The boundary voltage ≈ 950 μV is about 1/3 of the superconductor gap voltage for Nb-AlO_x-Nb tunnel junctions. To explain the experimentally measured I-V curves, a model based on self-coupling of Josephson radiation was introduced [32]. The effect of Josephson self-coupling (JSC) [36] is basically absorption of *ac* radiation by the quasi-particles in the cavity of the long junction. It is related to the well-known phenomenon of photon assisted tunneling (PAT). The JSC results in current bumps (similar to quasi-particle steps in a SIS mixer) at $V_{JSC} = V_g/(2n + 1)$, which gives $V_{JSC} = V_g/3$ for $n = 1$. The effect of self-pumping explains not only the current bumps observed in the FFO I-V curve, but also the abrupt merge of Fiske steps (absence of resonant modes at $V \geq V_g/3$). The reason is an increase of the internal damping in the long junction due to quasi-particle tunneling [32]. In other words, the geometric resonances (or FSs) may exist only for low normalized damping, $\alpha l < 1$ (where $l = L/\lambda_J$ is the junction length normalized to the Josephson penetration length λ_J). It worth to note that the resonant conditions can be satisfied even for a very long junction, $l = L/\lambda_J \geq 100$, if the damping is sufficiently low, say, $\alpha \leq 0.01$. According to theory, the FSs transforms into a smooth step similar to the Eck peak when the normalized damping increases to a value of about $\alpha l \geq 2$. This threshold depends on both length and initial damping. In accordance to qualitative calculations [32] the damping parameter becomes five times as large for $V > V_{JSC}$, and the FFO enters the "real" flux-flow regime where it is possible to continuously tune the frequency by the applied magnetic field.

3. FFO LINEWIDTH; PHASE LOCKING TO AN EXTERNAL OSCILLATOR.

The frequency resolution of a receiver (along with the noise temperature and the antenna beam pattern) is one of major parameters in spectral radio astronomy. The resolution which is determined by both the instantaneous linewidth of the local oscillator and its long-time stability should be much less than 1 ppm of the center frequency. Previous measurements of the linewidth of the FFO [21, 37-40] have demonstrated the following values; 130 kHz at 70 GHz [45], about 1 MHz at 280 GHz [21, 38], and 2.1 MHz at 320 GHz [39]. Recently a linewidth considerably below 1 MHz have been measured near 450 GHz [27]. Unique time resolved measurements of FFO radiation were performed by using an Acousto-Optical Spectrometer (AOS) with an integration time of 1 μs; and a linewidth of the free-running FFO less than 1 MHz at 350 GHz has been demonstrated [40]. However, the observed FFO linewidth is almost one order of magnitude wider [21, 38] than predicted by the theory for a *lumped* Josephson tunnel junction [42-44].

3.1 Experimental setup

The FFO linewidth was measured in a wide frequency range up to 600 GHz using a novel experimental technique [27]. A specially designed integrated circuit comprising the FFO, the SIS mixer, and the microwave circuit elements needed for the rf coupling is used for linewidth measurements (see figure 4). Both the SIS and the FFO junctions are fabricated from the same Nb-AlO_x-Nb trilayer, details have been described elsewhere [27, 32]. The signal from the FFO is applied to the harmonic mixer (SIS mixer operated in Josephson or quasiparticle mode) along with the signal from a reference frequency synthesizer, $f_{SYN} \approx 10$ GHz. In order to prevent the synthesizer signal (as well as its harmonics) from reaching the FFO a high-pass microstrip filter with a cut-off frequency of about 200 GHz is inserted between the FFO and the harmonic mixer.

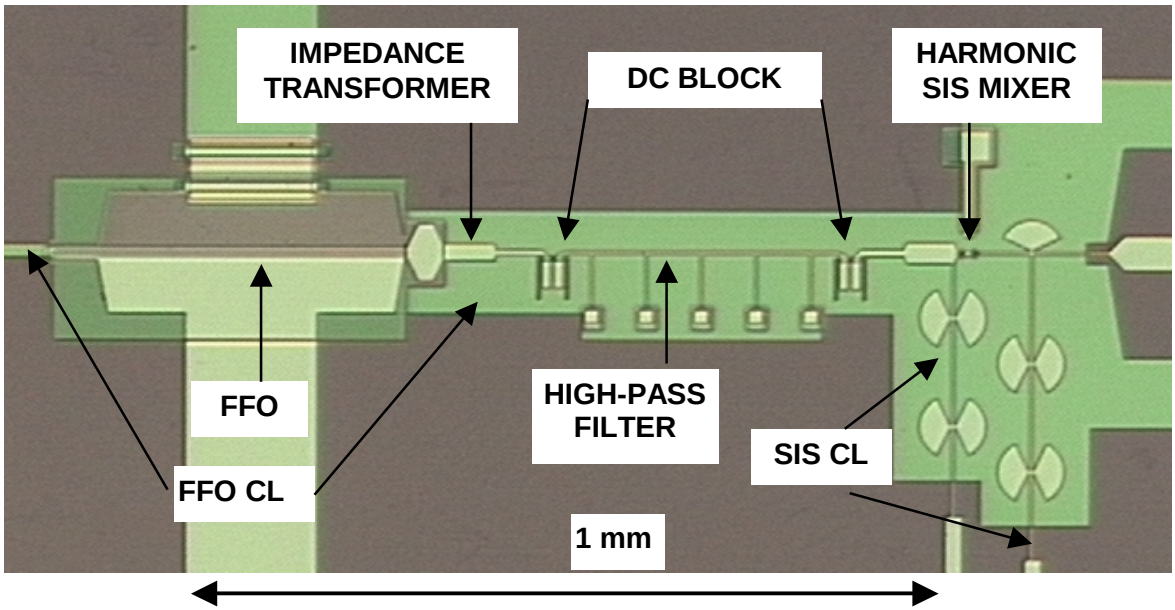

Fig. 4. Central part of the microcircuits used for FFO linewidth measurements.

A block diagram of the set-up for linewidth measurements is shown in figure 5. The intermediate frequency (IF) signal with frequency, $f_{IF} = \pm(f_{FFO} - n\, f_{SYN})$ is boosted first by a cooled amplifier ($T_n \approx 20$ K, gain = 27 dB gain) and then by a room temperature amplifier for use in the PLL system. A part of the signal is applied via the directional coupler to a spectrum analyzer which is also phase locked to the synthesizer using a common reference signal at 10 MHz. This down-converted spectrum of the FFO is presented in figure 6. Thus, the spectrum obtained at about 400 MHz, as well as the phase noise evaluated from these data, is the difference between the FFO signal and the *n*-th harmonic of the synthesizer.

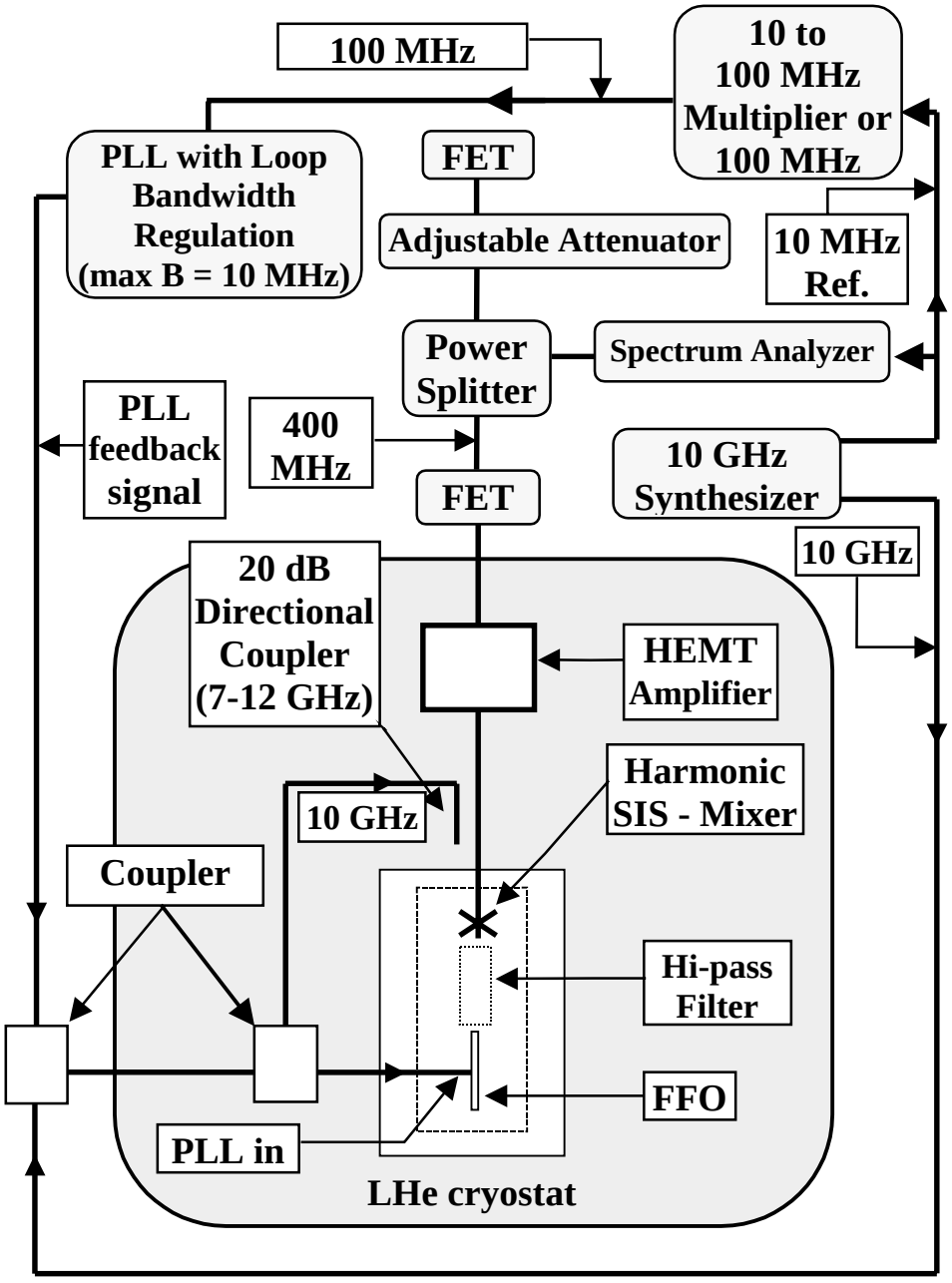

Fig. 5. [41] Block-diagram of the PLL circuit and set-up for linewidth measurement.

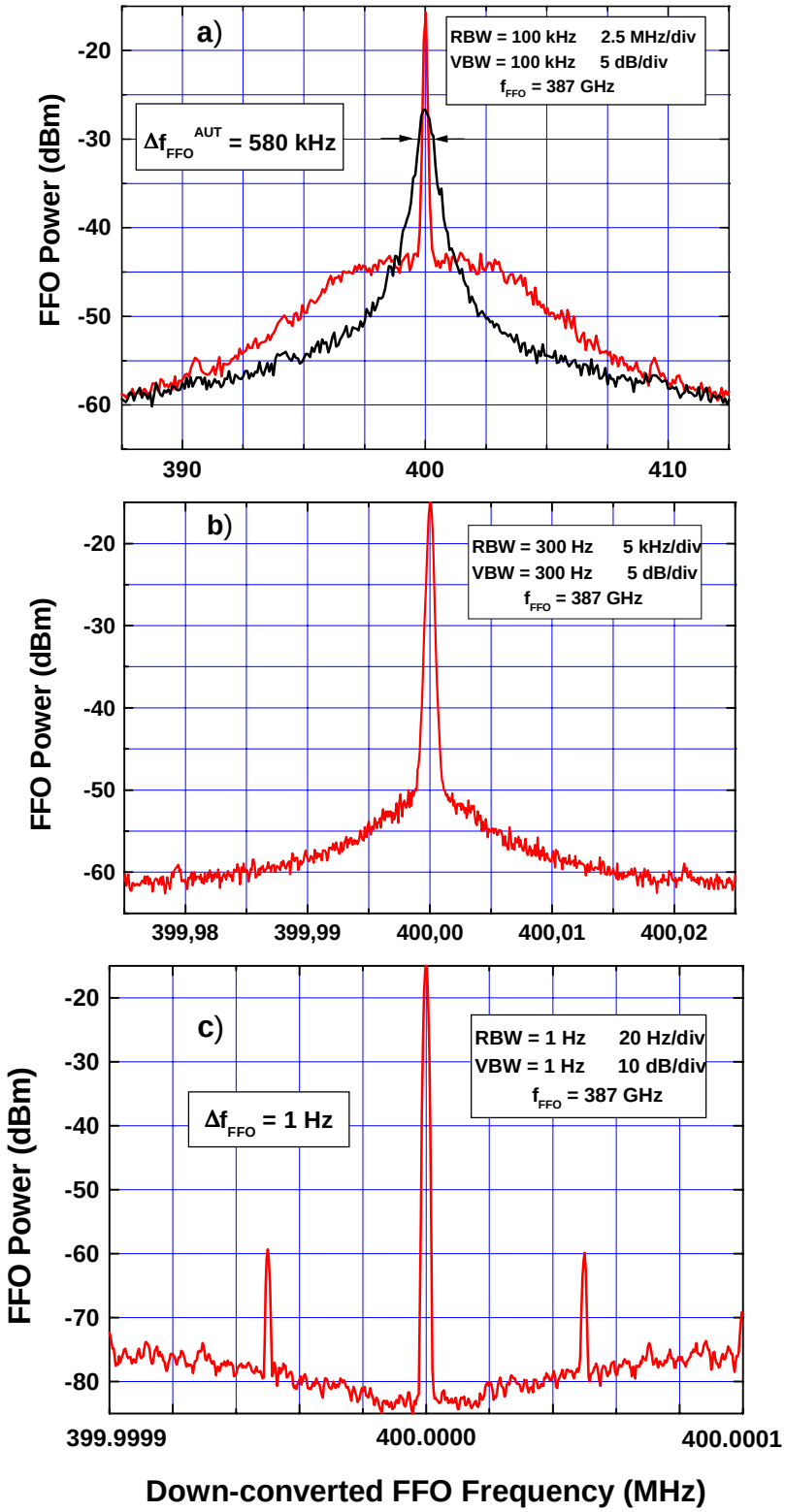

Fig. 6. [28] The down-converted IF power spectra of FFO (f = 387 GHz) recorded with different frequency spans clearly demonstrate the phase locking to within 1 Hz relative to the reference oscillator.

In the PLL unit the intermediate frequency ≈ 400 MHz is divided by four and compared in a Frequency-Phase Discriminator with a 100 MHz reference signal (also phase locked to the main 10 GHz synthesizer). The output signal proportional to the phase difference is returned via the Loop Bandwidth Regulator (maximum bandwidth about 10 MHz) and then fed-back to the FFO via a coaxial cable terminated with cold 50 Ω resistor mounted on the chip bias plate. The results of FFO phase locking to an external reference oscillator will be discussed in detail in the Section 3.4.

In order to perform accurate linewidth measurement of a free-running FFO, the IF spectra have to be averaged with a sufficiently narrow video bandwidth. The PLL system with a relatively low loop gain and narrow bandwidth setting (< 10 kHz) can be used for *frequency locking* of the FFO in order to measure the linewidth, Δf_{AUT}, of the free-running FFO. In this case it is assumed that drift and only very low frequency noise are eliminated by the narrow-band feedback. Thus the linewidth, determined by the much faster fluctuations, which are assumed to be the "natural" ones, can be carefully measured.

The integrated harmonic mixer may be operated in two different modes: quasiparticle and Josephson. In order to realize a pure quasiparticle regime the Josephson supercurrent has to be suppressed by a magnetic field. In the present design this is done by applying a current ($I_{SIS}CL$) via the SIS control line, see figure 4. As a matter of fact, no significant difference between these two regimes has been found at proper power settings of the synthesizer power, see figure 7. Note, that a much higher power is required in the quasiparticle regime. The FFO output signal is about 6 dB higher for the Josephson regime ($I_{SIS}CL$ =0), but the signal to noise ratio is the same (the curve for quasiparticle regime is shifted upwards by 6 dB for better comparison). On the other hand, the spectrum measured in the quasiparticle regime has smaller phase noise, which may be important for future applications.

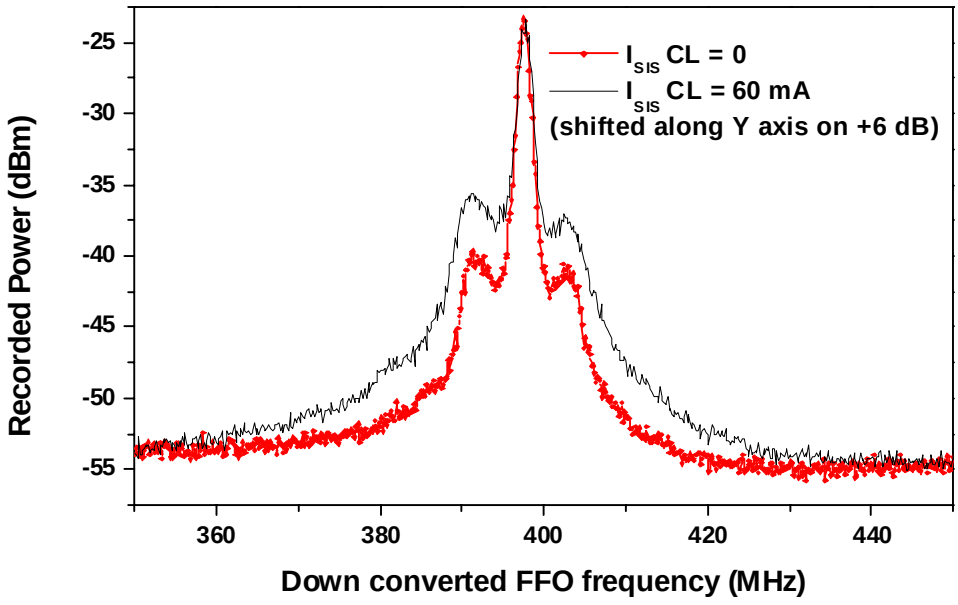

Fig. 7. Comparison of the Josephson ($I_{SIS}CL$ = 0) and quasiparticle operational regimes of the integrated harmonic mixer.

3.2. Super-fine structure of the FFO IVCs; External Harmonic Multiplier.

Accurate FFO linewidth measurements [27, 45] have allowed us to detect a superfine structure of closely spaced resonances with a frequency separation of ≈10 MHz. The fine structure manifests itself as a highly nonlinear relation between the measured FFO frequency and the FFO bias or/and control-line currents. In order to exclude that the recorded resonance structure could be due to the integrated harmonic mixer technique, an external harmonic multiplier based on a quasi-planar superlattice electronic device (SLED) [46] has been developed and tested [47, 48]. The SLED was mounted in a circular waveguide with a cut-off frequency of about 400 GHz followed by a conical horn with an output diameter of 6 mm. A constant-voltage bias and the pump signal from the synthesizer (frequency 5 - 22 GHz) were applied to the SLED. The signal of the multiplier was fed to an integrated receiver of standard design [1, 24] via a vacuum window (see figure 8). Heterodyne mixing with the FFO local oscillator signal can be measured up to 500 GHz corresponding to the 27-th harmonic of the input signal from the synthesizer ($f_S \approx$ 18 GHz). Figure 9 shows the down-converted FFO signals measured by this technique with the FFO frequency locked (curve A) and phase locked (curve B), respectively.

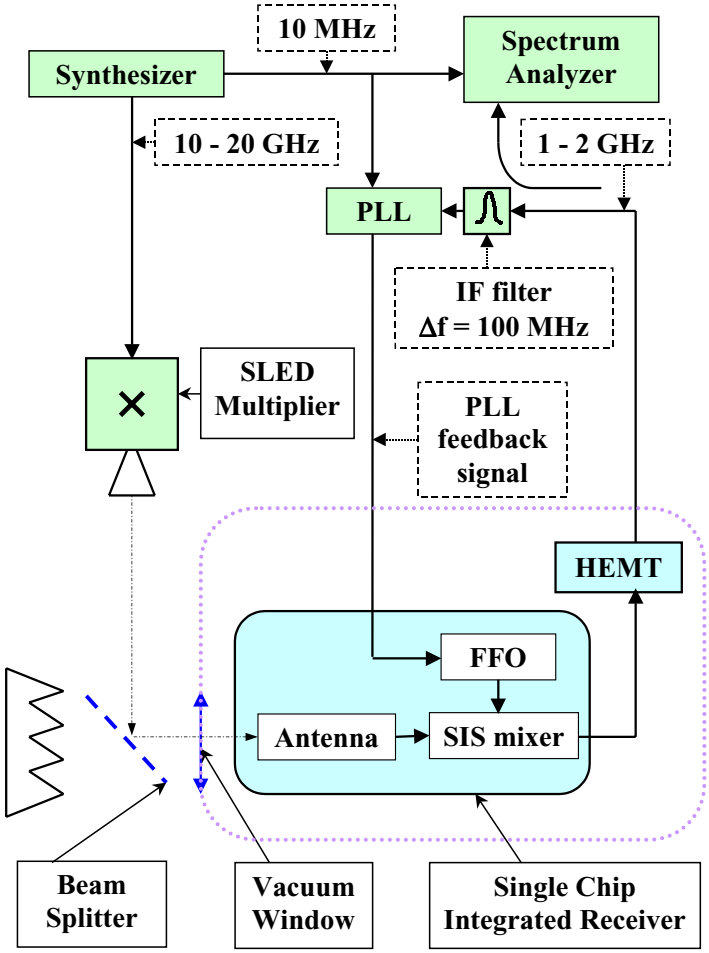

Fig. 8. Block Diagram of the Superconducting Integrated Receiver (SIR) with phase locked FFO and external harmonic multiplier (SLED, see text).

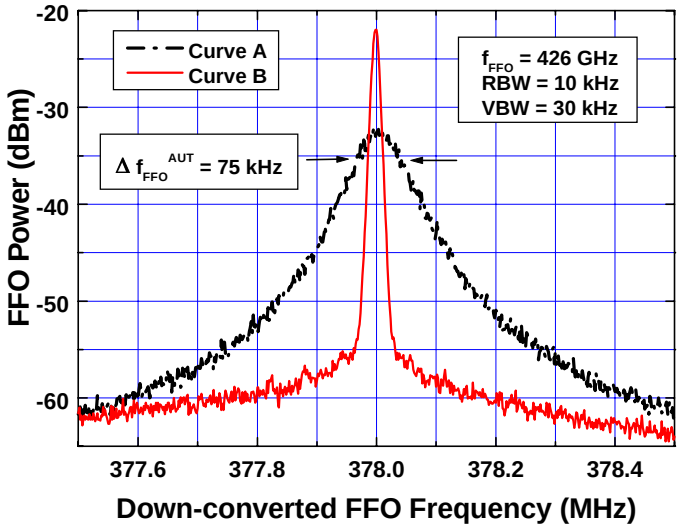

Fig. 9. Down-converted spectra of the FFO operated at 426 GHz with the FFO frequency locked (curve A) and phase locked (curve B) using the external SLED harmonic mixer.

The superfine resonance structure is present also in the measurements made with the external multiplier, and thus the resonances can be attributed to properties of the FFO rather than to the measuring method. Generally an FFO can irradiate only in a specific frequency range near the corresponding "resonance" frequencies, f_r, while it is unstable between these values. This behavior is clearly demonstrated in figure 10. Traces A and B are recorded at two constant bias currents: I_B = 17 782 μA and 17 779 μA, point A and B respectively (number of measurements averaged, N_{av} = 100). Point A is almost stable while an attempt to bias at point B fails due to the small fluctuations which force the FFO to rapidly jump between stable states, spending on the average almost equal time in both states (curve B).

Trace "C" in figure 10 illustrates this phenomenon in a different way. It is recorded when fine-tuning the FFO bias (from 18 710 μA to 18 770 μA) in the "max-hold" regime. In this regime the spectrum analyzer takes the maximum signal amplitude from many measurements at each frequency point. One can see that the FFO frequency can be continuously tuned only in a range of about 5 MHz, while frequencies between these stable regions cannot be obtained. Even a small change of the bias current near the edge of the stable region will result in a "jump" of the FFO voltage (frequency) to the next stable region.

Using the Josephson equation the FFO IVC can be reconstructed in detail by measuring the FFO output frequency versus bias current. The accuracy of the frequency (and correspondingly, the voltage) measurement is determined by the spectrum analyzer resolution used. For the data presented in figure 10 and 11 the resolution bandwidth, RBW, was 300 kHz corresponding to a voltage accuracy of about 0.6 nV. By using a special measuring procedure the frequency reading from the spectrum analyzer could be recorded while simultaneously adjusting I_B and I_{CL}. From these data the exact shape of the FFO IVC can be reconstructed. The "recovered" FFO IVCs demonstrate the existence of a well-defined superfine structure (see figure 11). The voltage spacing is about 20 nV, which is somewhat below the resolution of usual dc technique.

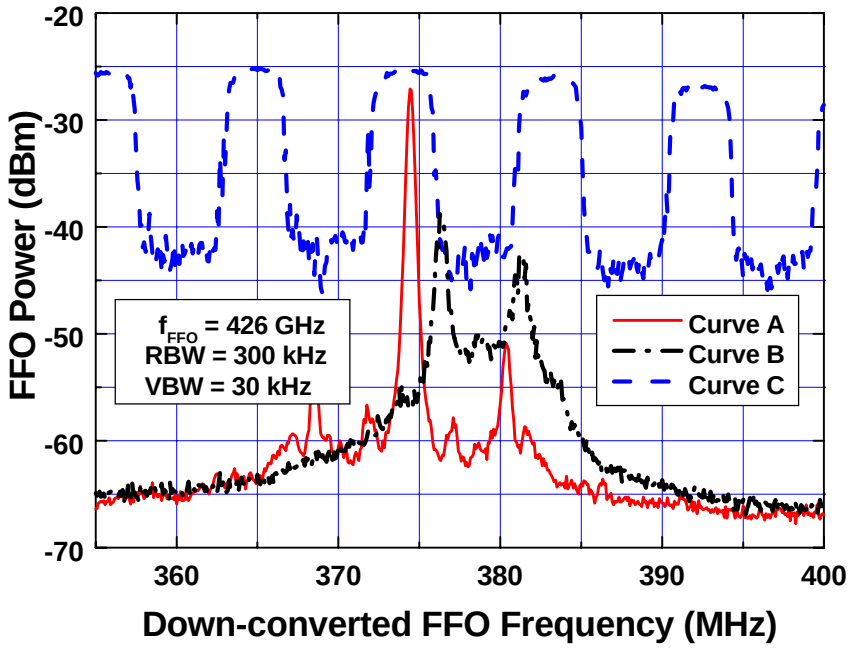

Fig. 10. Down-converted FFO signal recorded at constant bias current adjusted inside one of the resonances (curve A) and in between two resonances (curve B). Curve C is recorded with the FFO bias tuned in the "max-hold" regime.

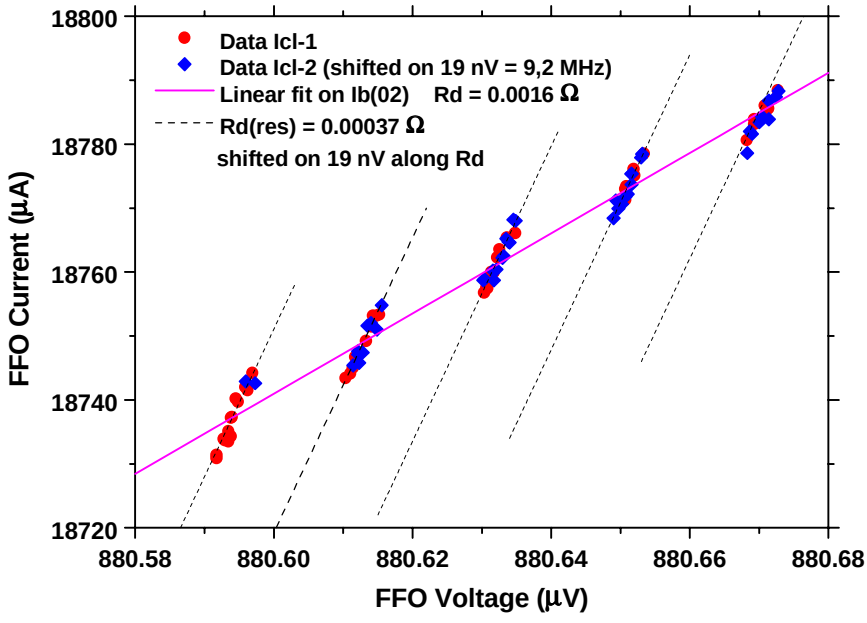

Fig. 11. Reconstructed IVC of the FFO. Data marked "I_{CL}-*2*" are measured at a slightly different I_{CL} value and corresponds to adjacent resonance. The hatched lines shifted by 19 nV along the Fiske step with slope $1/R_d^B$.

From figure 11 one can see that the FFO IVC consists of a series of separate steps rather than being a continuous curve. The differential resistance $R_d^B = \partial V/\partial I_B$ on these steps is extremely low, R_d^B(res) = 0.00037 Ω. It is important to note that this value is considerably lower than the average value (R_d^B = 0.0016 Ω) found with the traditional dc technique. An even more dramatic reduction has been measured for the control-line differential resistance, $R_d^{CL} = \partial V_{FFO}/\partial I_{CL}$ (0.0009 Ω and 0.0073 Ω respectively). Obviously, this step structure can easily be smeared out at higher levels of interference from external noise sources.

Note that the very narrow linewidth ≈75 kHz (figure 9, curve A) was measured at a FFO frequency of 426 GHz in a bias point with extremely low differential resistance. Actually, this is the linewidth of the free-running FFO since it was recorded with a very narrow (< 10 kHz) PLL regulation bandwidth that only suppresses low-frequency external interference without changing the FFO linewidth (frequency locking).

Since the frequency separation between adjacent resonances is comparable to the maximum bandwidth of the PLL system, jumps between adjacent resonances create considerable difficulties for phase locking of the FFO. Nevertheless full phase locking can be realized even in the presence of the resonance structures, but only in certain frequency ranges (see figure 9). At lower temperatures (T < 4.2 K) the resonant structure becomes more pronounced and even more tightly spaced steps can be observed.

Up to now no theoretical explanation has been given of this superfine resonant structure. The exact geometry of the FFO influences the resonant structure. In particular, the results reported in [28] were measured for a FFO with variable width where the resonance effect was less pronounced. The results depicted in figures 10, 11 are from a FFO with standard rectangular overlap geometry. In order to confirm that the resonance structure is related to the FFO geometry and can be avoid by optimization of the FFO layout we have developed a new design of the FFO (HD7, see figure 12).

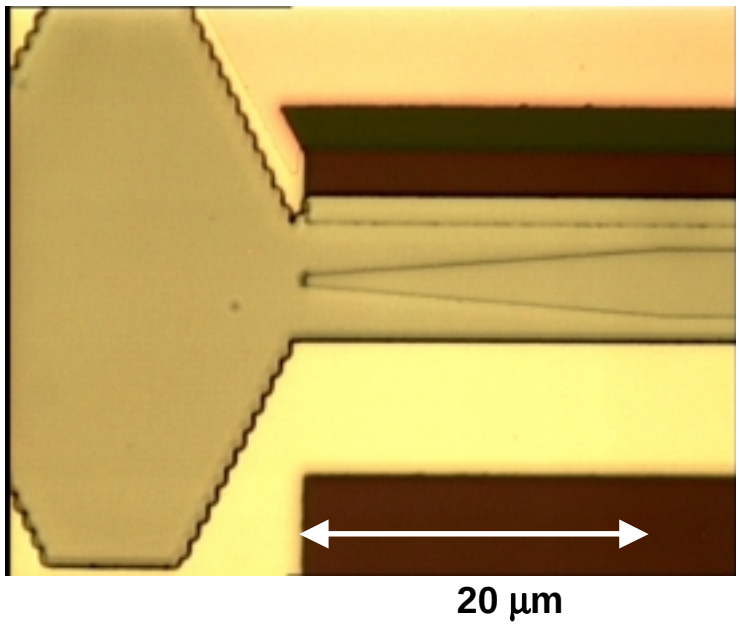

Fig. 12. Photo of the central part of the HD7 circuit showing one end of the tapered FFO and the first stage of the impedance transformer.

In this design the FFO is tapered from both sides so that its width is decreased from 6 μm to 1.5 μm over a distance of 20 μm. As a result of this modification the resonant structure was almost totally suppressed, see figure 13 (data were measured by an integrated SIS harmonic mixer). In this figure continuous frequency tuning is demonstrated by curve B. This curve is recorded providing a fine-tuning of the FFO bias in the spectrum analyzer "max-hold" regime (compare to curve "C" in figure 10). One can see that the FFO frequency can be continuously adjusted over the whole FFO frequency tuning range, which in the figure is limited by a spectrum analyzer span of 50 MHz. The small variations of the maximum level is due to non-ideal coupling between the SIS mixer and the coolable IF amplifier (standing waves). It should be noted that a tapered FFO has larger output impedance as compared to a standard FFO of rectangular shape. This considerably simplifies the impedance matching to the following microwave circuits. At the left end of the FFO one can see the first section of the impedance transformer, which loads the FFO output.

Only at specific conditions a reminiscence of the resonant structure has been observed for the new FFO (figure 14). This structure results in an appearance of the small bumps on the FFO emission line profile, nevertheless continuous frequency tuning was possible, see figure 14, curve "B". These peaks resemble the effect of a weak modulation of the sinusoidal signal. From figure 14 one can see three non-equidistant bumps on each side of the FFO line. The reason for this extra modulation is under investigation. Note that the figures 13 and 14 have been recorded in experiments with the same sample. Possibly it may be associated with a minor influence of the Abrikosov' vortices trapped so far from the FFO that they do not significantly modify the FFO characteristics.

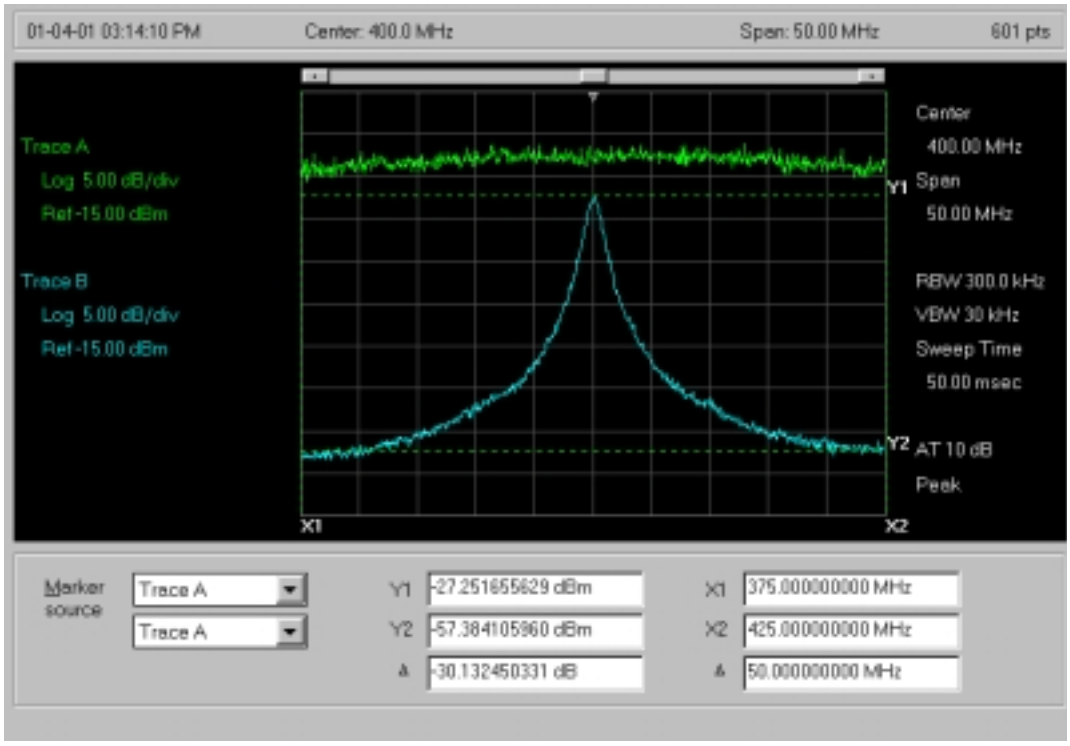

Fig. 13. Down-converted FFO signal recorded at constant bias current (curve A). Curve B is recorded with the FFO bias tuned in the "max-hold" regime.

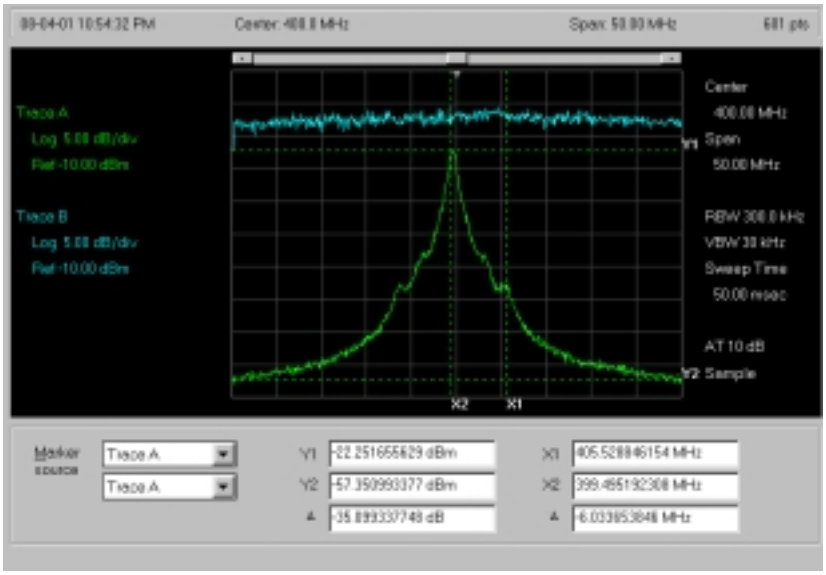

Fig. 14. Down-converted FFO signal recorded at constant bias current (curve A). Note the small non-equidistant bumps on both sides of the FFO line. Curve B is recorded with the FFO bias tuned in the "max-hold" regime.

3.3. Linewidth of the FFO: theory and experiment.

Presently no well-established theory exists for the FFO linewidth, but preliminary estimations can been done [41] on the basis of the general theory for the radiation linewidth of the *lumped* Josephson tunnel junction [42 - 44]. The linewidth, δf, of a Josephson junction is mainly determined by low frequency current fluctuations. For white noise it can be written (see e.g. [44]) as:

$$\delta f = (2\pi/\Phi_0^2)\,(R_d^B)^2\, S_i(0), \qquad (1)$$

where $S_i(0)$ is the power density of the low frequency current fluctuations, $R_d^B = \partial V/\partial I_B$ is the dc differential resistance which transforms the current fluctuations to voltage (and phase) noise.

For a lumped tunnel junction [43, 44]

$$S_i(0) = (e/2\pi)\,\{I_{qp}\coth(v) + 2\,I_s\coth(2v)\}, \quad \text{with} \quad v = (eV_{dc})/(2\,k_B\,T_{eff}), \qquad (2)$$

where k_B is Boltzmann's constant. I_{qp}, I_s and V_{dc} are respectively the quasiparticle current, superconducting current and averaged dc voltage in the bias point. T_{eff} is the effective temperature of the quasiparticles in the junction electrodes. This formula describes a nonlinear superposition of thermal and shot noise. The supercurrent itself cannot be a source of fluctuations because of its reactive character; the additional term proportional to I_S appears due to the interaction of the supercurrent with the embedding circuit. It should be noted that formula does not take into account the spatial variation of the tunnel current along the FFO, the interactions of the moving fluxons, and the influence of the external low frequency interference. All these effects are believed to increase the FFO linewidth. Nevertheless, very recently it was shown [49] that a formula similar to Eq. (2) can be applied for a distributed LJJ in the limit where there are many fluxons in the junction.

Fluctuations in the external magnetic field (which affect the average distance between fluxons) can be accounted for by the differential tuning resistance of the control line $R_d^{CL} = \partial V_{FFO}/\partial I_{CL}$ for fixed dc bias current I_B. In the case of an *external interference* both the "usual" differential resistance R_d^B and R_d^{CL} "convert" low frequency external noise currents, $I_{lf}^{(B, CL)}$, to frequency fluctuations following the same relations:

$$\delta f \propto R_d^{(B, CL)} * I_{lf}^{(B, CL)}. \qquad (3)$$

A numerical model of the FFO based on expressions (1) – (3) and taking into account the thermal noise from the biasing resistors, as well as external low frequency interference via the bias and control line circuitry has been developed [41]. It was shown [41] that the thermal noise in the biasing resistors is negligible small in a well designed bias and control line circuitry. The radiation linewidth for different models of the noise contributions calculated using measured FFO parameters are presented in figure 15 as a function of the differential resistance R_d^B. Curve 1) is calculated using the standard tunnel junction model [43, 44], which describes a nonlinear superposition of thermal and shot white noise, Eqs. (1) and (2). In this model δf is proportional to $(R_d^B)^2$. Curve 2) is calculated taking into account only low frequency external fluctuations via the bias current leads, Eq. (3), I_{lf} =0.1 μA. Curves 3) and 4) include both white noise and external fluctuations. The external fluctuations via both bias and control line current leads are calculated for two different R_d^{CL} values: $R_d^{CL}1$ = 0,002 Ω - typical for resonant regime on FS (curve 3), and $R_d^{CL}2$ = 0,1 Ω in the flux-flow regime for $V > V_{JSC}$ (curve 4). One can see that the FFO linewidth at $R_d^B < 0.011$ Ω is mainly determined by fluctuations coming from the control line.

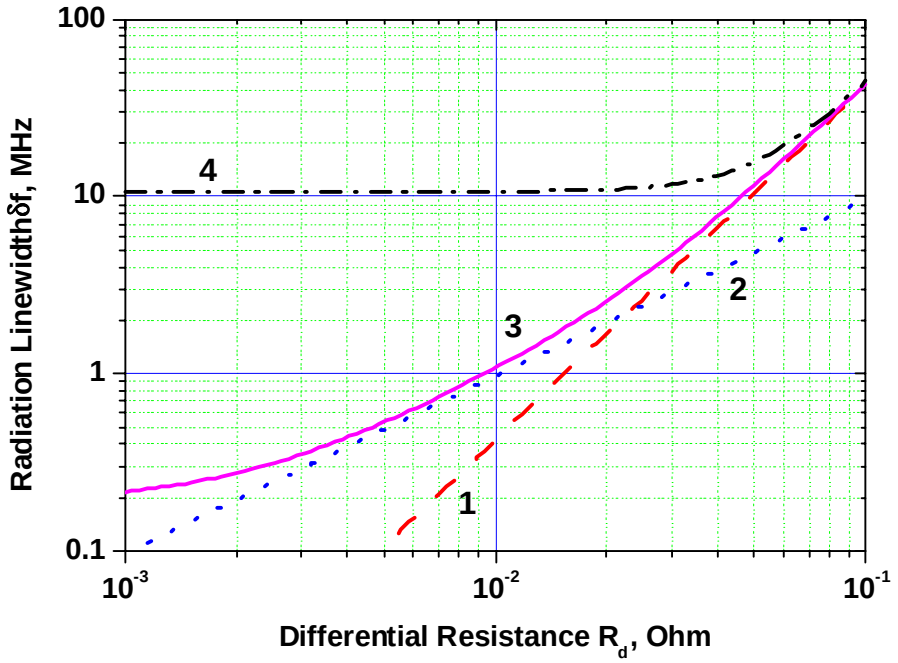

Fig. 15. Calculated dependence of the radiation linewidth δf on the differential resistances R_d for typical FFO parameters: T_{eff} = 4.2 K, V_{dc} = 1 mV, I_{qp} = 2.5 mA, I_s = 7.5 mA, I_{lf} = 0.1 μA (see text for details).

The results presented in figure 15 demonstrate the importance of the R_d^{CL} value: even in the simple FFO model for quite low levels of the external low frequency fluctuations (I_{lf} = 0.1 μA) the radiation linewidth is as large as 10 MHz in the flux flow regime for $V > V_{JSC}$. Previous experiments [32, 41] have shown a significant increase of the radiation linewidth for large values of the differential resistance as compared to the linewidth calculated from Eqs. 1-3, see curves 3) and 4) in figure 15. This significantly complicates the phase locking of the FFO in this regime. In order to reduce both the bias and control line differential resistances a new design of the FFO electrodes has been made. A photo of the central part of the new design of the FFO is shown in figure 16. The control line is realized as a separate strip in an additional superconducting layer.

Typical IVCs of the FFO with new design measured using the data acquisition system IRTECON are shown in figure 17. Note that both differential resistances are considerably reduced (compare with figure 1, where the control line current range was about 20 mA). The dependence of the FFO critical current on magnetic field produced by the control line current is shown in figure 18 for two samples with different control line design. The solid circles present the data measured for the geometry shown in figure 16, while the open diamonds are for the same FFO employing the base electrode as a control line. One can see that the curves are almost identical except for the fact that the scale of the control line current is almost three times larger. This means that R_d^{CL} has been reduced by a factor 3. Results of direct measurements of the dependence of the FFO voltage on I_{CL} at three different bias currents are presented in figure 19 (data are collected using the IRTECON system). Note that polarities of I_{CL} are opposite for these two cases due to the design of the separate control line.

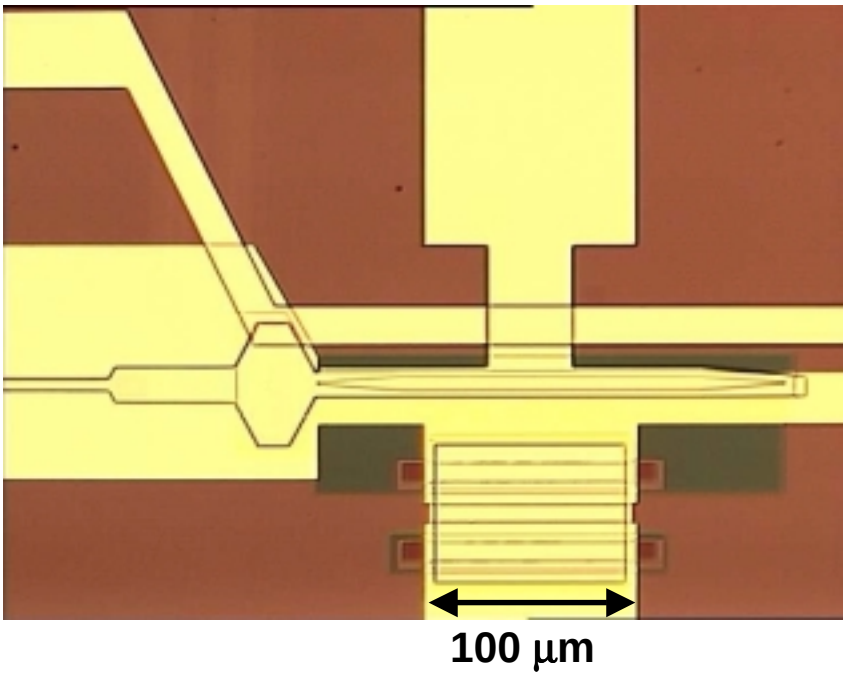

Fig. 16. Photo of the FFO of HD7 design. One can see a tapered FFO with the bias resistor placed below FFO, the separate control line (on top of the FFO), and the impedance transformer on left side.

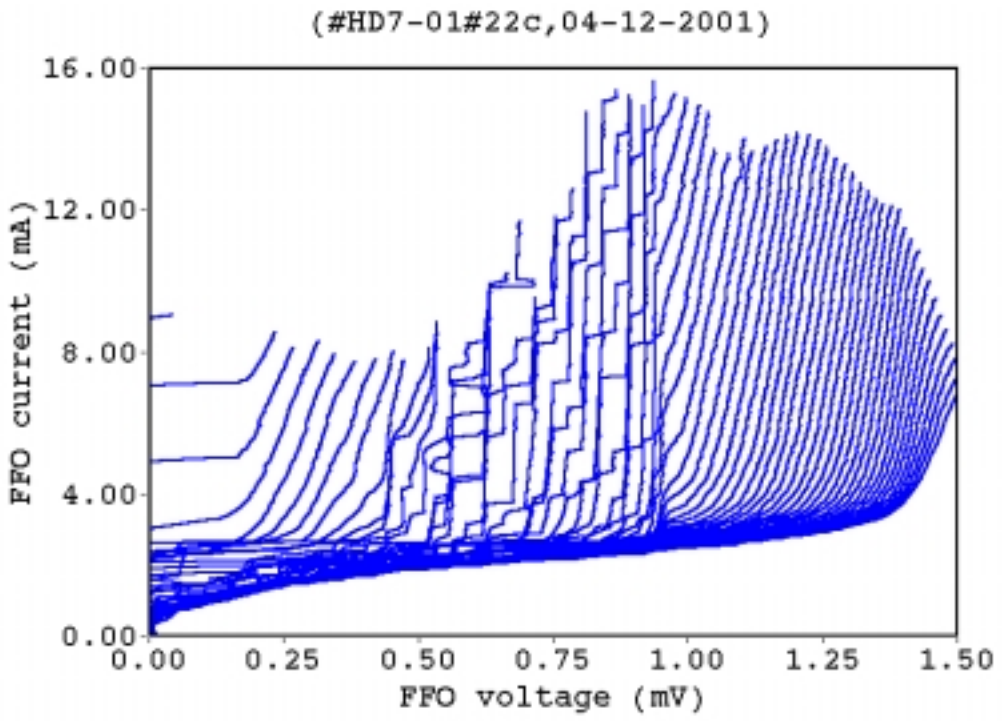

Fig. 17 IVCs of a FFO with new design (HD7) measured by the data acquisition system IRTECON at different control line currents (from 20 to 80 mA in steps of 1 mA).

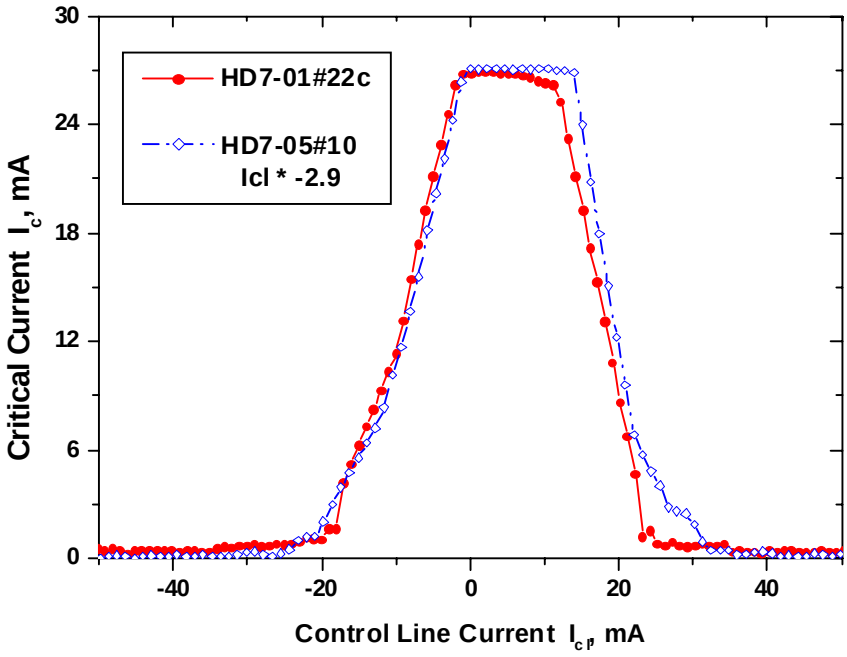

Fig. 18. Dependence of the critical current I_c on the control line current I_{CL} for a FFO with separate control line – solid circles. Similar dependence for the FFO of exactly the same geometry employing the base electrode as control line is shown for comparison by open diamonds. Note that for this curve I_{CL} is multiplied by a factor of –2.9.

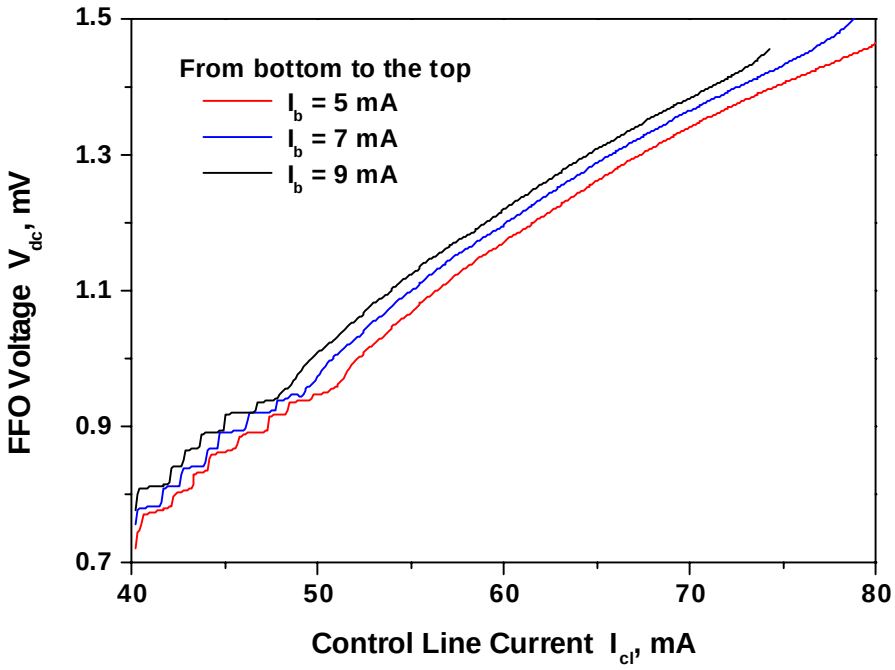

Fig. 19. Dependence of the FFO voltage on the control line current at 3 different bias currents: I_B = 5, 7 and 9 mA.

As a result of all these modifications a FFO radiation linewidth of about 10 MHz has been measured in the whole flux flow regime: from 490 to 630 GHz, see figure 20. This provides the possibility of phase locking the FFO also for $V > V_{JSC}$ (see Section 3.4).

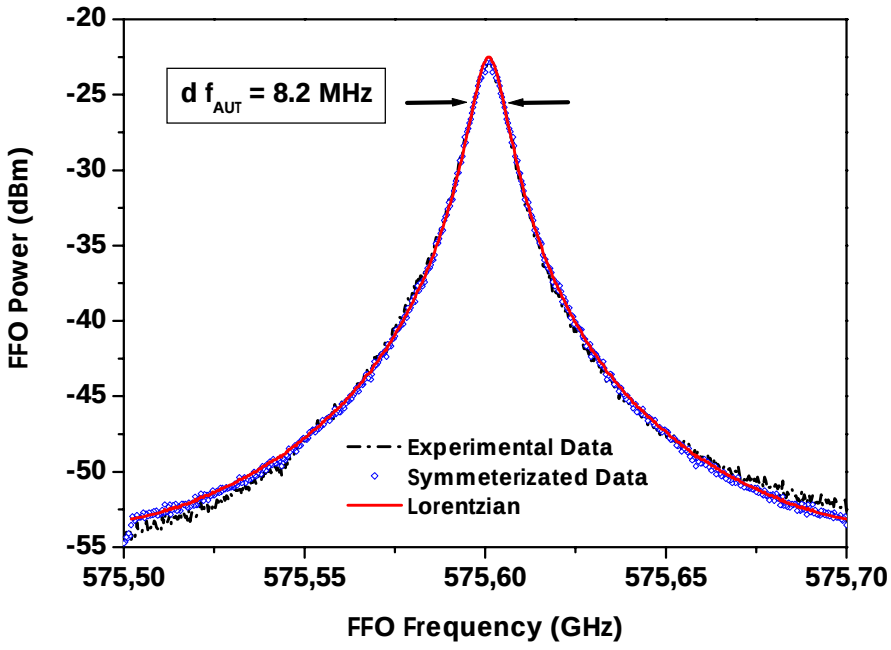

Fig. 20. Down-converted spectra of the FFO frequency locked at 576 GHz.

The absence of the resonance structure makes it possible to perform a detailed analysis of the spectrum of radiation emitted by the free-running FFO. The shape of the FFO spectrum provides important information about both the internal and the external fluctuations and the related parameters. A frequency detection system with a relatively low loop gain has been used to frequency lock the FFO to an external reference oscillator. In this case it is assumed that only low-frequency noise and drift are eliminated by the narrow-band feedback. Thus the linewidth, determined by much faster internal fluctuations, which are assumed to be the "natural" ones, can be carefully measured. An example of the FFO spectrum measured on the Flux Flow Step (FFS) is presented in figure 20 by dash-dotted line. The measured data are symmetrizated relative to the center frequency; these data are shown by diamonds. According to theory [44, 50] the spectral distribution will be Lorentzian (L) for wide- band fluctuations, which is the case for the pure flux-flow regime on the FFS with large differential resistance R_d^B (see figure 15 and the corresponding discussion). The calculated Lorentzian is shown in figure 20 as the solid line. The coincidence between the calculated curve and the symmetrizated experimental data is excellent, actually better than 5% in the emitted power if a minor amplifier's nonlinearity of about 0.4 dB is taken into account.

The profile of the FFO line recorded when biased at the steep Fiske step (FS), where the differential resistance is extremely small, can be different from the one measured on the smooth Flux Flow step. Theoretically [44, 50] the shape is Lorentzian for wide-band fluctuations, while for narrow-band interference, at frequencies smaller than the autonomous FFO linewidth δf_{AUT}, the profile will be Gaussian. The FFO spectrum measured at the Fiske step is presented in figure 21; the theoretical curves are also shown in figure 21 for comparison. The theoretical lines providing the best fit near the peak are shown by the solid line and the dashed line for Lorentzian and Gaussian, respectively.

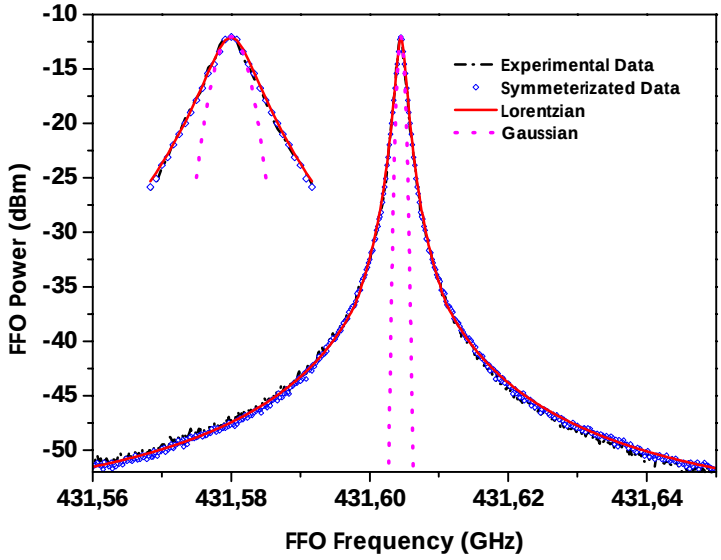

Fig. 21. FFO spectrum measured when biased on the Fiske step (V_{FFO} = 893 μV, R_d = 0.0033 Ω, R_d^{CL} = 0.00422 Ω, δf_{AUT} = 1.2 MHz) – dash-dotted line. The symmetrizated experimental data are shown by diamonds. Fitted theoretical Lorentzian and Gaussian profiles are shown by solid and dotted lines, respectively. The inset shows a zoom-in on the central peak with the frequency axis multiplied 5 times.

The FFO line shape is very well approximated by the Lorentzian expression. For some experimental conditions a small deviation – so-called "wings" - has been recorded, which can be accounted for by adding a second "broader" Lorentzian component. Such line shape with "wings" is typical [50] for an oscillator affected by both frequency and amplitude fluctuations. Furthermore, according to [50], the minor asymmetry of the measured FFO line profile can be ascribed to correlations between frequency and amplitude fluctuations, which is to be expected at the steep Fiske step. At higher voltages on the FFS, the asymmetry is even more pronounced (see figure 20).

The data in figure 21 demonstrate that even at extremely low differential resistance R_d^B the emission line profile is Lorentzian; even at the "plateau" of curve 3) in figure 15 at $R_d^B < 0.01\ \Omega$. This fact is very important for linewidth calculations. It gives us experimental evidence that the wide-band fluctuations are present in the magnetic field, because according to [41] at small R_d^B the FFO linewidth is mainly determined by fluctuations of the magnetic field. Since an influence of the wide-band fluctuations in the biasing resistors feeding the control line (CL) is negligibly small [41], it means that there must be a channel for transfer of the wide-band fluctuations from the bias current I_B to the FFO via the magnetic field. Partially, it can be associated with a self-field effect (part of the bias current is flowing along the FFO electrodes creating a magnetic field proportional to I_B). Under these circumstances the role of the differential resistance of the CL, $R_d^{CL} = \partial V_{FFO}/\partial I_{CL}$, becomes even more important. This has never been taken into account in the theoretical considerations. If we include the wide-band fluctuations via the CL in the numerical model [41] by an empirical coefficient K (as a multiplier to the measured value of R_d^{CL}), this allows us to fit the experimental linewidth data to the calculated both on the Fiske steps and on the flux flow step (see figure 22).

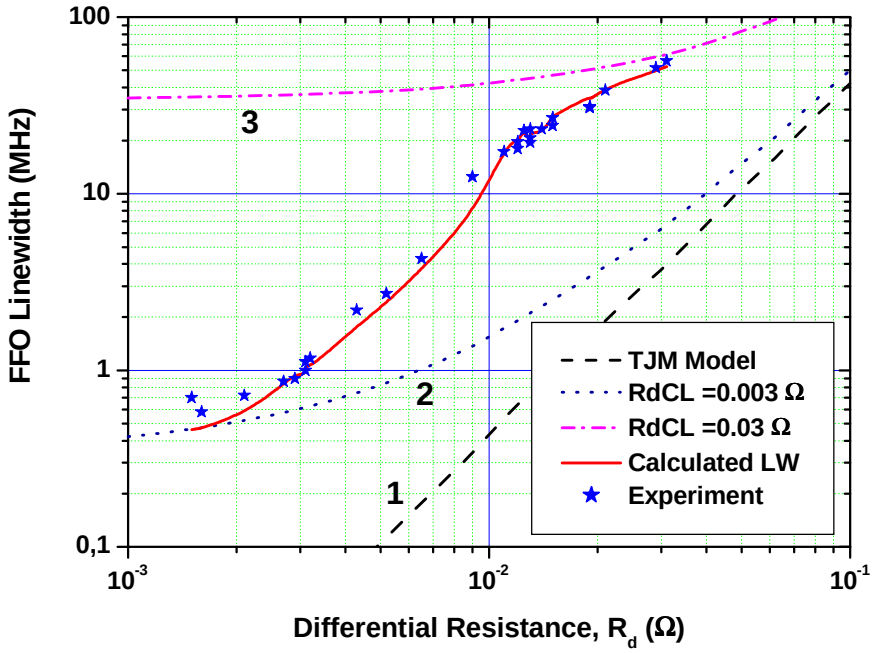

Fig. 22. Dependence of the FFO radiation linewidth on the differential resistance R_d (see text). Curves 1 - 3 are calculated for the following experimental parameters: V_{dc}= 1 mV, I_{qp}=3 mA, I_s=7 mA, T_{eff} = 4.2 K.

Since the fluctuations via the magnetic field are generated by wide-band fluctuations in the bias current, the correlation between this two noise components must be taken into account. This results in the following expression for the FFO linewidth:

$$\delta f = (2\pi/\Phi_0^2)\,(R_d^B + K{*}R_d^{CL})^2\, S_i(0). \qquad (4)$$

This empiric expression seems to be very similar to the formula derived recently by A. Pankratov [51] on the base of the same assumption concerning the influence of wide-band fluctuations via magnetic filed.

The calculated dependence of the linewidth of lumped tunnel junction [43, 44] for the case of wide-band fluctuations only via I_B (K = 0) is shown in figure 22 by the dashed line 1), the dependence for fixed values of R_d^{CL} = 0.003 Ω and R_d^{CL} = 0.03 Ω are presented by the dotted and the dash-doted lines 2) and 3), respectively. The solid line is calculated for each experimental point taking into account all measured parameters (I_B, V, R_d^{CL}, etc.). One can see that the calculations coincide with the measured linewidth data over the whole range of experimental parameters by using only one value of K =2.9 both on the Fiske steps and on the flux flow step. The agreement between the calculations Eq. (4) and the experimental data plotted as a function of the bias current at two different values of the CL current is also very good (see figure 23). These values of the CL current correspond to two different regimes of FFO operation: at the Fiske step (I_{CL} = 45 mA) and on the flux flow step (I_{CL} = 50 mA), again the same value of K = 2.9 is used for all calculations. The exact value of K depends on the specific FFO design; data from figures 22, 23 are measured for a design with the separate CL presented in figure 16. In this case the ratio between the currents, flowing on the separate CL and through the base electrode and producing the same magnetic field, is equal to 2.9 (see figure 18). This indicates that the bias current in total adds the noise contribution via the magnetic field, but this should be studied further by special experiments.

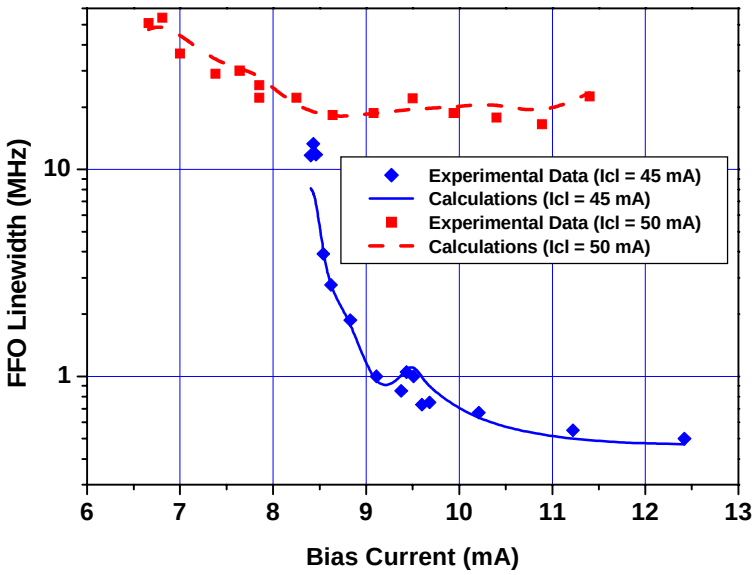

Fig. 23. Dependence of the FFO radiation linewidth on the bias current for two values of the CL current (45 mA – at the Fiske step; 50 mA – on flux flow step). Solid lines represent the data calculated according to Eq. (4).

3.4. FFO Phase locking and its Phase Noise

According to this theoretical consideration the radiation linewidth is determined by both the differential resistance of the FFO and the noise spectral density at low frequencies, $0 < f < \delta f_{AUT}$, where δf_{AUT} is the free-running FFO linewidth. The FFO is a voltage-controlled oscillator and hence its frequency can be stabilized and the FFO linewidth can be decreased by locking to an external reference oscillator using a phase-lock loop (PLL) system with bandwidth larger than δf_{AUT}. Actually, a PLL system will effectively alter both the spectral density of the external low frequency fluctuations and the differential resistances associated with the bias and control line tuning. These resistances transform current fluctuations into voltage (frequency) fluctuations according to Eqs. (3) and (4).

For the traditional FFO design the free-running linewidth δf_{AUT} for $V > V_{JSC}$ is considerably larger than the regulation bandwidth of conventional PLL systems (< 1 MHz). This makes it almost impossible to phase lock a FFO on the flux flow step where the FFO frequency can be continuously tuned. A new FFO design (figure 16) provides a free-running FFO linewidth of about 10 MHz or smaller at all frequencies of interest. Besides a special ultra-wide-band PLL system (regulation bandwidths of about 30 MHz) has been developed. As a result, the FFO has been phase locked up to 630 GHz (see figure 24a). Note that a relative FFO linewidth as low as 1 Hz has been achieved at this high frequency and with a relatively large signal to noise ratio, SNR (figure 24b). At lower FFO frequencies on Fiske steps, where the free-running linewidth δf_{AUT} is considerably smaller, an even better residual phase noise has been realized (figure 25).

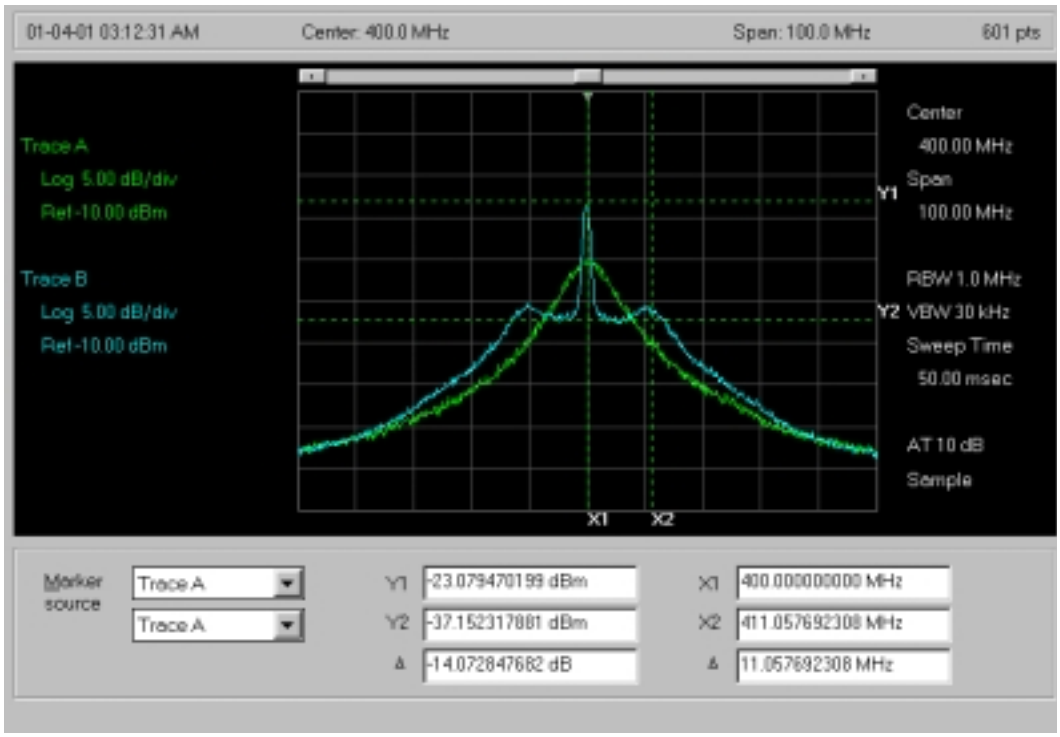

Fig. 24a. Down converted spectra of frequency locked (A) and phase locked FFO (B), operating at 633 GHz. The free-running linewidth was δf_{AUT} = 8.4 MHz.

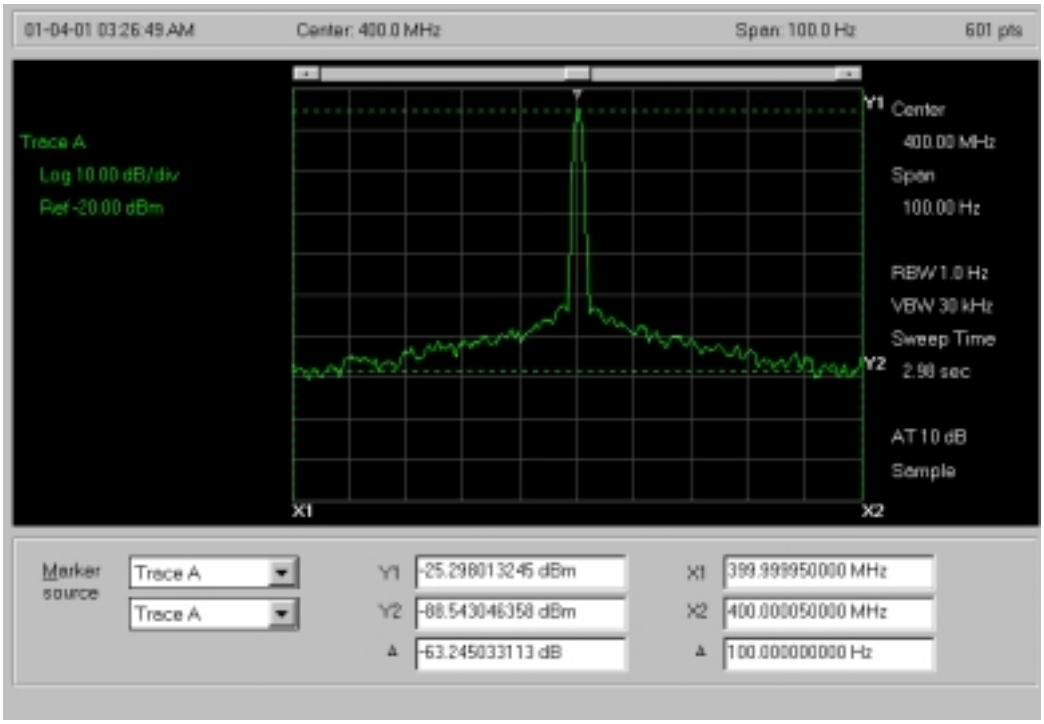

Fig. 24b. Down converted spectra of the phase locked FFO operating at 633 GHz. Note the 1 Hz linewidth and the 63 dB signal to noise ratio.

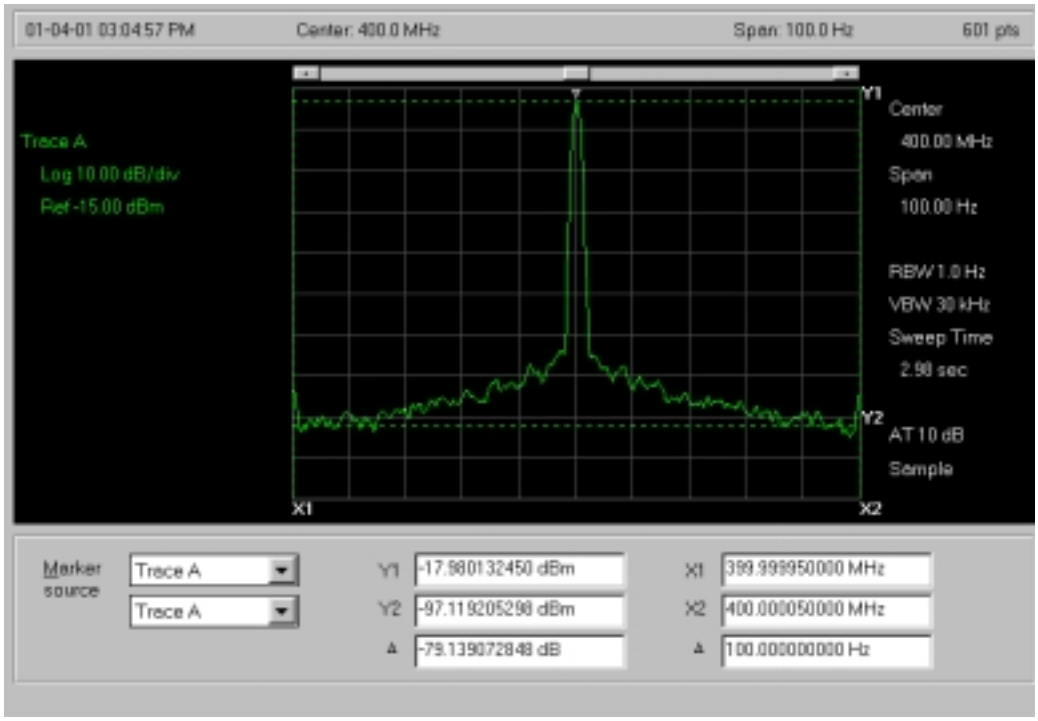

Fig. 25. Down converted spectra of phase locked FFO, operating at 444 GHz. Note the 1 Hz linewidth and the 79 dB signal to noise ratio.

The residual phase noise of the phase locked FFO - measured relative to the reference oscillator (high quality synthesizer) - is plotted in figure 26 as function of the frequency offset from the carrier. The data are presented for two different FFO regimes of operation, in the resonant regime biased on a Fiske step and on the soft flux flow step. Note that there is no pronounced dependence of the phase noise on the frequency in either of the two regimes. The difference between the two regions is mainly due to larger initial linewidth and lower SNR on the flux flow step. A similar increase of the phase noise was measured on parts of a Fiske step with larger R_d^B and R_d^{CL} values. In order to get the absolute phase noise of the phase locked FFO, one should add the synthesizer noise multiplied by n^2 (n is the harmonic number) to the measured residual phase noise of the FFO. In this particular measurement where the FFO, operating at 444 GHz, is locked to the 24-th harmonic of the synthesizer operating at 18.5 GHz, $n^2 = 576$. The measured data for the synthesizer (HP83752B) are also presented in figure 26. The absolute FFO phase noise (solid line in figure 26) is dominated by the synthesizer noise for offsets < 1 MHz. The slight increase of the noise at larger frequency offsets is mainly due to the PLL system, which adds some noise at frequencies close to its regulation bandwidth.

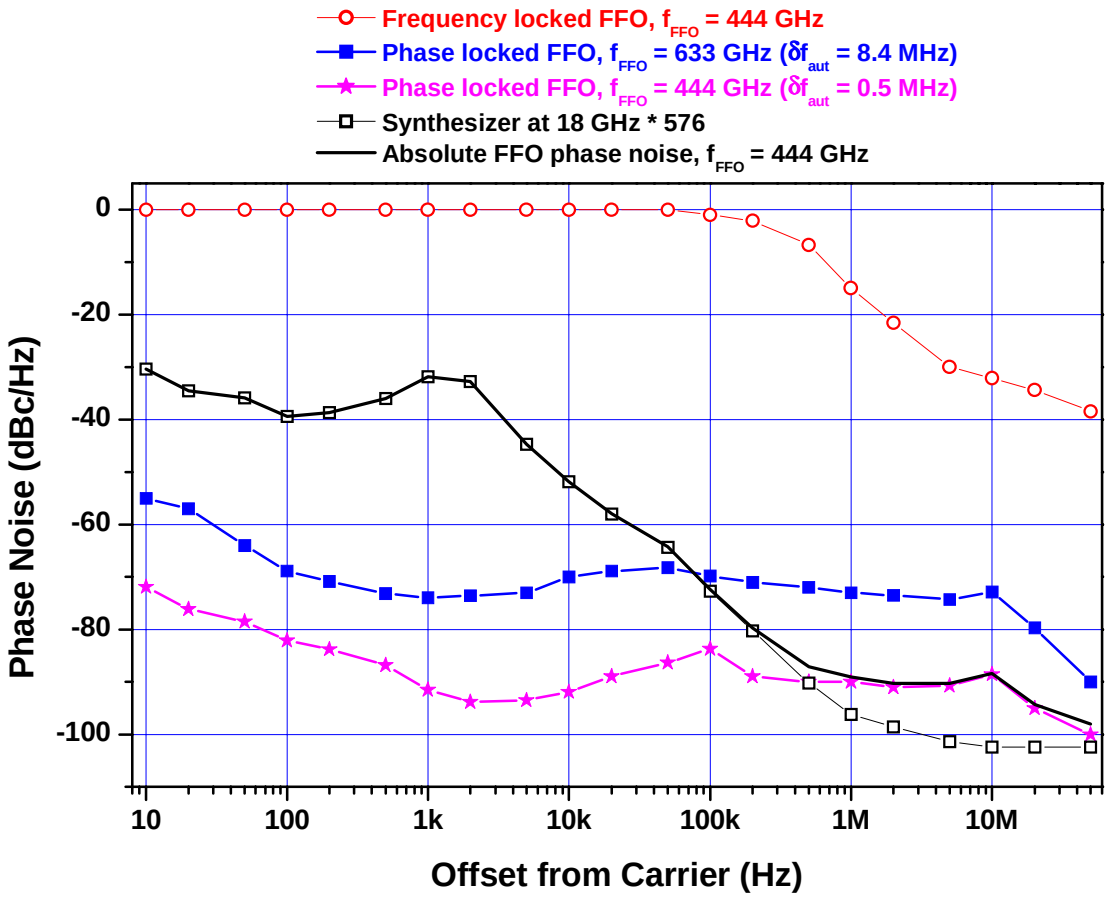

Fig. 26. Experimental phase noise of a phase locked FFO at different frequencies. Since the phase noise of the FFO, e.g., at 444 GHz is measured relative to the 24th harmonic of the synthesizer, the synthesizer noise, multiplied by a factor $24^2 = 576$, should be added to the residual FFO noise to get the total (absolute) FFO phase noise – solid line.

3.5 Towards the phase locked Superconducting Integrated Receiver

The combination of narrow linewidth and wide-band tunability makes the FFO a perfect on-chip local oscillator for an integrated submm receiver for spectral radio astronomy and aeronomy applications. Implementation of the single-chip Superconducting Integrated Receiver (SIR) for new radio-astronomy projects based on a multi-receiver approach (e. g., ALMA) is especially advantageous as compared to the conventional SIS receiver with external Gunn oscillator and multipliers. It is important to note that ultimate performance of the SIR is basically the same as for the best waveguide and quasi-optical SIS receivers in the frequency range of 400 - 600 GHz where SIRs have been tested up to now. Both the wide-band tunability, the convenience of simple electronic control of the FFO local oscillator and the low weight and price make the SIR very attractive compared to existing SIS receivers. The data given above clearly demonstrate the feasibility of an electronic control of frequency and power of the FFO along with the possibility of narrowing the linewidth of the Josephson oscillator using an external PLL system, provided that the PLL bandwidth is larger than the intrinsic linewidth δf_{AUT} of the free-running oscillator.

Recent results on phase locking of an FFO to an external reference oscillator have been used to develop the practical concept of the integrated receiver with phase-locked loop [41, 52] presented schematically in figure 27. Following this concept a 350 GHz receiver chip containing a quasioptical SIS mixer, a phase-locked flux flow oscillator, a harmonic SIS mixer and an SIS multiplier as a source for the harmonic mixer (optional) has been designed, fabricated and pre-tested recently [52]. The FFO is phase-locked to the 35th harmonic of a 10 GHz synthesized source using custom-design room temperature electronics with a PLL loop bandwidth of about 10 MHz.

The external harmonic multiplier enables us to check an alternative concept of the Phase Locked Integrated Receiver. This concept is based on an already proven design of the integrated receiver chip [1], [24]. In this approach a submm-wave signal from an external harmonic multiplier driven by a 10 - 20 GHz synthesizer is applied to the integrated receiver via a beam splitter (see figure 8 for details). A small portion of the IF band (about 50 MHz) is used to monitor the mixing product between the n-th harmonic of the synthesizer signal and the FFO signal. This down-converted signal after narrow-band filtering controls the phase locking loop (PLL) system while the rest of the IF band is used to analyze the down-converted signal. Here the development of a cryogenic multiplier looks very promising. The output power may be increased according to theoretical expectations, and a much thicker beam splitter can be used at cryogenic temperatures due to the reduced contribution to the receiver noise temperature.

The present state of development of the PLL Integrated Receiver for practical spectral radio astronomy is, so far, quite encouraging. The receiver contains well-understood elements and devices and is under the test in the frequency range 350-450 GHz. In this frequency range the Fiske steps (FS) of the Nb-AlO_x-Nb FFO are closely spaced and almost overlapping due to the low junction losses and the dispersion in the long Josephson tunnel junction [35]. The frequency gaps between the available LO bands corresponding to the voltage difference between subsequent FSs, where FFO phase locking is possible, do not exceed 5 GHz for the chosen FFO length. One may cover these gaps by using a wide-band IF amplifier with wide enough bandwidth (2-4 GHz) to allow continuous frequency coverage while the FFO is biased and locked on adjacent FSs.

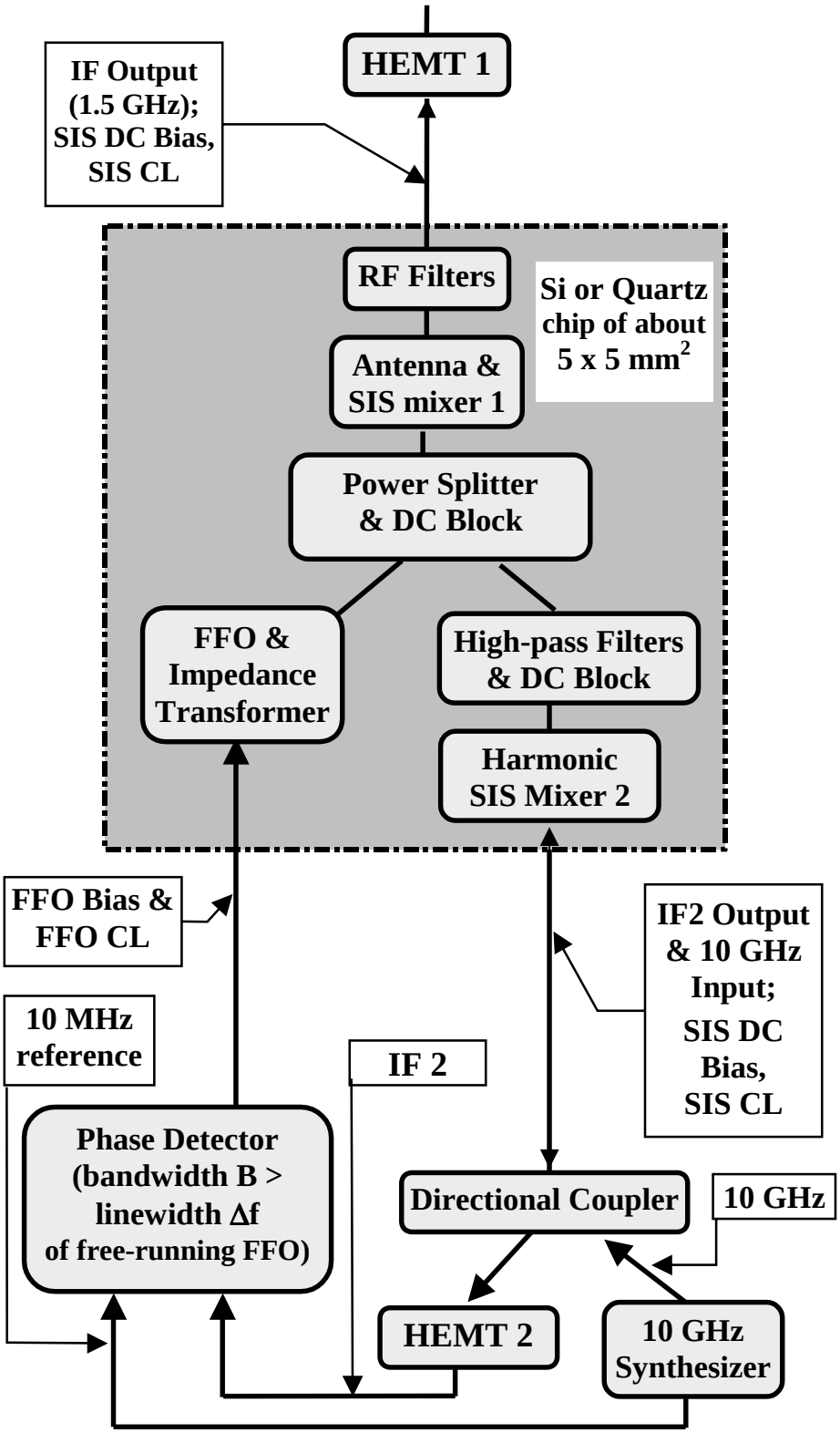

Fig. 27. Block-diagram of the sub-millimeter all-superconducting phase locked single-chip Integrated Receiver. The common FFO pumps two SIS mixers, one serves as the detector/mixer, and the other facilitates the phase locking of the FFO.

4. CONCLUSIONS

A review of the main properties of the superconducting local oscillator based on long Josephson junction is presented. All reported data demonstrate that flux flow oscillators are already well developed for integration with SIS-mixers in a single-chip all-superconducting submillimeter wave receiver (SIR). The integrated receivers fabricated on niobium trilayer, $Nb/AlO_x/Nb$, are proven to be useful within the frequency range 100-700 GHz showing noise temperatures better than 1 K/GHz which is comparable to the performance of 'traditional' SIS receivers with external fixed-frequency phase locked local oscillators (LO). The antenna beam properties obtained for the integrated receiver are satisfactory for use on a real radio telescope. An imaging array receiver based on 9 integrated receiver pixels employing elliptical silicon optics is being tested and shows no essential degradation of the pixel performance. The concept of the on-chip PLL integrated receiver is currently subjected to intensive experimental study.

Acknowledgement.

The work was supported in parts by the Russian SSP "Superconductivity", the RFBR projects 00-02-16270, INTAS project 97-1712, ISTC project # 1199, the Netherlandse Organisatie voor Wetenshappelijk Onderzoek (NWO) grant, the Danish Natural Science Foundation, and the Hartmann Foundation. Authors deeply appreciate the participation in the development and study of the Flux Flow Oscillators for Integrated Receiver by all members of the large international team, especially Andrey Baryshev, Andrey Ermakov, Lyudmila Filippenko, Pavel Dmitriev, Viktor Khodos, Dimitry Paveliev, Alexander Sobolev, Sergey Shitov and Vladimir Vaks. Authors thank Thijs de Graauw, Willem Luinge, Mikhail Khapaev, Michael Kupriyanov, Andrey Pankratov, Mario Salerno, Mogens R. Samuelsen, Herman van de Stadt, Alexey Ustinov, Paul Wesselius, Nick Whyborn, Wolfgang Wolf and Alexey Yulin for fruitful and stimulating discussions as well as H. Golstein, S. Kikken, H. Smit and D. Van Nguyen for help in the experiment.

References

[1] V.P. Koshelets and S.V. Shitov, Superconductor Science and Technology, **13** (2000) R53.

[2] J.R. Tucker and M.J. Feldman, *Rev of Mod Phys*, **4** (1985) 1055.

[3] R. Blondel and C.E. Tong, *Proc IEEE*, **80** (1992) 1702.

[4] J. Carlstrom and J. Zmuidzinas, in Review of Radio Science 1993-1996, edited by W.R. Stone, Oxford University Press, Oxford (1996) 839.

[5] S.V. Shitov, V.P. Koshelets, S.A. Kovtonyuk, An.B. Ermakov, N.D. Whyborn, and C-O. Lindstrom, *Supercond Sci Technol*, **4** (1991) 406.

[6] A. Karpov, J. Blondel, M. Voss and K.H. Gundlach, *IEEE Trans on Appl Superconductivity*, **5** (1995) 3304-7; A. Karpov, B. Plathner, and J. Blondel, *IEEE Trans on Appl Superconductivity*, ***7*** (1997) 1077.

[7] J. Zmuidzinas and H.G. LeDuc, *IEEE Trans on Microwave Theory and Tech.*, **40** (1992) 1797; J. Zmuidzinas, N.G. Ugras, D. Miller, M.C. Gaidis, H.G. LeDuc and J.A. Stern, *IEEE Trans on Appl Superconductivity*, **5** (1995) 3053; M.C. Gaidis, H.G. LeDuc, Mei Bin, D. Miller, J.A. Stern and J. Zmuidzinas, *IEEE Transactions of Microwave Theory and Techniques*, **44** (1996) 1130.

[8] S. Han, B. Bi, W. Zhang and J.E. Lukens, *Appl Phys Lett*, **64** (1994) 1424.

[9] S. Kiryu, W. Zhang, S. Han, S. Deus S, and J.E. Lukens, *IEEE Trans App Supercond*, **7** (1997) 3107; S. Deus and S. Kiryu, *IEEE Trans App Supercond.*, **9** (1999) 4325.

[10] P.A.A. Booij and S.P. Benz, *Appl Phys Lett*, **68** (1996) 3799.

[11] A. Kawakami and Z. Wang, *IEICE Trans Electron.*, **E-61C** (1998) 1595.

[12] A. Kawakami, Y. Uzawa and Z. Wang, *IEEE Trans App Supercond.*, **9** (1999) 4554.

[13] H.S.J. van der Zant and T.P. Orlando, *J Appl Phys*, **76** (1994) 7606.

[14] M.J. Wengler, B. Guan and B. Track, *Microw Theory Tech*,. **43** (1995) 984.

[15] P.A.A. Booij and S.P. Benz, *Appl Phys Lett*, **64** (1994) 2163.

[16] P. Caputo, A.V. Ustinov, N.C.H. Lin and S.P. Yukon, *IEEE Trans Appl Supercond.*, **9** (1999) 4538.

[17] J. Oppenlinder, W. Guttinger, T. Traeuble, M. Kerk and T. Doderer, *IEEE Trans Appl Supercond.*, **9** (1999) 4337.

[18] P. Barbara, A.B. Cawthorne, S.V. Shitov and C.J. Lobb, *Phys Rev Lett*, **82** (1999) 1963.

[19] V.P. Koshelets, S.V. Shitov, A.V. Shchukin, A.M. Baryshev, L.V. Filippenko, G.M. Fisher and J. Mygind, *Appl Phys Lett*, **63** (1993) 3218.

[20] T. Nagatsuma, K. Enpuku, F. Irie, and K. Yoshida, *J Appl Phys*, **54** (1983) 3302, see also Pt. II: *J Appl Phys* **56** (1984) 3284; Pt III *J Appl Phys* **58** (1985) 441; Pt IV *J App. Phys* **63** (1988) 1130.

[21] J. Mygind, V.P. Koshelets, A.V. Shchukin, S.V. Shitov and I.L. Lapytskaya, *IEEE Trans on Appl Supercond*, **5** (1995) 2951.

[22] V.P. Koshelets, S.V. Shitov, A.M. Baryshev, I.L. Lapytskaya, L.V. Filippenko, H. van de Stadt, J. Mess, H. Schaeffer and T. de Graauw T, *IEEE Trans on Appl Supercond.*, **5** (1995) 3057.

[23] V.P. Koshelets, A.V. Shchukin, S.V. Shitov and L.V. Filippenko, *IEEE Trans on Appl Supercond.*, **3** (1993) 2524.

[24] V.P. Koshelets, S.V. Shitov, L.V. Filippenko, A.M. Baryshev, H. Golstein, T. de Graauw, W. Luinge, H. Schaeffer and H. van de Stadt, *Appl Phys Lett* **68** (1996) 1273.

[25] V.P. Koshelets, S.V. Shitov, L.V. Filippenko, A.M. Baryshev, A.V. Shchukin, G.V. Prokopenko, P.G. Litskevitch, T. de Graauw, W. Luinge, H. van de Stadt, H. Golstein, H. Schaeffer, T.M. Klapwijk, J-R. Gao, P. Lehikoinen and J. Mygind, Proceedings of 30-th ESLAB Symposium *ESTEC the Netherlands*, (1996) 193

[26] S.V. Shitov, A.B. Ermakov, L.V. Filippenko, V.P. Koshelets, A.M. Baryshev, W. Luinge, J-R. Gao, *IEEE Trans on Appl Supercond.*, **9** (1999) 3773.

[27] V.P. Koshelets, S.V. Shitov, L.V. Filippenko, A.V. Shchukin, and J. Mygind, *Appl Phys Lett*, **69** (1996) 699.

[28] V.P. Koshelets, S.V. Shitov, L.V. Filippenko, V.L. Vaks, J. Mygind, A.B. Baryshev, W. Luinge and N. Whyborn, *Rev of Sci Instr.*, **71** (2000) 289.

[29] A.B. Ermakov, S.V. Shitov , A.M. Baryshev, V.P. Koshelets, W. Luinge, Applied Superconductivity Conference ASC'2000, September (2000), Report 4EA10; *IEEE Trans. on Appl. Supercond.*, **v.11,** No 1, pp. 840-843, (2001).

[30] S. Kohjiro and A. Shoji, presented at *EUCAS'99 Barcelona Spain* September report 6-103 (1999); Inst. Phys. Conf. Ser. No 167, Vol. 2, pp.655-658, IOP Publishing Ltd (2000)

[31] V.P. Koshelets, S.V. Shitov, L.V. Filippenko, A.M. Baryshev, W. Luinge, H. Golstein, H. van de Stadt, J-R. Gao and T. de Graauw, *IEEE Trans on Appl Supercond*, **7** (1997) 3589.

[32] V.P. Koshelets, S.V. Shitov, A.V. Shchukin, L.V. Filippenko, J. Mygind and A.V. Ustinov, *Phys Rev B,* **56** (1997) 5572.

[33] G.S. Lee, *IEEE Trans on Appl Supercond,* **3** (1991) 121; N. Thyssen, A.V. Ustinov, H. Kohlstedt, S. Pagano, J.G. Caputo and N. Flytzanis, *IEEE Trans on Appl Supercond.,* **5** (1995) 2965.

[34] A.V. Ustinov, H. Kohlstedt, and P. Henne, *Phys Rev Lett,* **77 (**1996) 3617.

[35] M. Cirillo, N. Gronbech-Jensen, M.R. Samuelsen, M. Salerno and G. Verona Rinati, *Phys Rev B,* **58** (1998) 12377.

[36] L.-E. Hasselberg, M.T. Levinsen and M.R. Samuelsen, *Phys Rev B,* **9** (1974) 3757.

[37] A.V. Ustinov, T. Doderer, R.P. Huebener, J. Mygind, V.A. Oboznov, and N.F. Pedersen, *IEEE Trans on Appl Supercond.,* **3** (1993) 2287.

[38] V.P. Koshelets, A.V. Shchukin, I.L. Lapytskaya, and J. Mygind, *Phys Rev B,* **51 (**1995) 6536.

[39] Y.M. Zhang, D. Winkler, and T. Claeson, Appl Phys Lett, **62** (1993) 3195.

[40] U. Muller and K. Jacobs, *Proceedings of the 10th International Symp on Space Terahertz Techn.,* Clarlottesville, USA (1999) 13.

[41] V.P. Koshelets, S.V. Shitov, A.V. Shchukin, L.V. Filippenko, P.N. Dmitriev, V.L. Vaks, J. Mygind, A.B. Baryshev, W. Luinge and H. Golstein, *IEEE Trans on Appl Supercond.,* **9** (1999) 4133.

[42] M.J. Stephen, *Phys Rev,* **182** (1969) 531.

[43] A.J. Dahm, A. Denenstein, D.N. Langenberg, W.H. Parker, D. Rogovin, and D.J. Scalapino, Phys Rev Lett, 22 (1969) 1416.

[44] K.K. Likharev, "Dynamics of Josephson junctions and circuits" *Gordon and Breach Science Publishers* (1986).

[45] A.V. Ustinov, private communication.

[46] E. Schomburg, R. Scheuerer, S. Brandl, K.F. Renk, D.G. Paveliev, Yu. Koschurinov, V. Ustinov, A. Zhukov, A. Kovsh and P.S. Kop`ev, *Electronics Letters,* **35** (1999) No 17.

[47] V.P. Koshelets, A.B. Ermakov, S.V. Shitov, P.N. Dmitriev, L.V. Filippenko, A.M. Baryshev, W. Luinge, J. Mygind, V.L. Vaks and D.G. Pavel'ev, Proceedings of the 11th International Symposium on Space Terahertz Technology, University of Michigan, Ann Arbor. May 1-3, (2000) 532.

[48] V.P. Koshelets, A.B. Ermakov, S.V. Shitov, P.N. Dmitriev, L.V. Filippenko, A.M. Baryshev, W. Luinge, J. Mygind, V.L. Vaks and D.G. Pavel'ev, Applied Superconductivity Conference ASC'2000, September (2000), Report 5EG06; *IEEE Trans. on Appl. Supercond.,* **v.11,** No 1, pp. 1211-1214, (2001).

[49] M. Salerno, M.R. Samuelsen, and A. Yulin, Phys Rev Lett, 86 (2001) 5397

[50] A.N. Malakhov, "Fluctuations in auto-oscillating systems", Science, Moscow, 1968 (in Russian).

[51] A.L. Pankratov, "Form and width of spectral line of Josephson Flux-Flow oscillator", arXiv:cond-mat/0105387, to be published.

[52] S V. Shitov, V. P. Koshelets, L. V. Filippenko, P. N. Dmitriev A. M. Baryshev, W. Luinge and J.-R. Gao, *Proc. of 10th Int. Symp. on Space Terahertz Techn.,* Clarlottesville, USA (1999) 447.